

## **Noroviruses subvert the core stress granule component G3BP1 to promote viral VPg-dependent translation.**

### **Authors:**

Myra Hosmillo<sup>1\*</sup>, Jia Lu<sup>1\*</sup>, Michael R. McAllaster<sup>2\*</sup>, James B. Eaglesham<sup>1,3</sup>, Xinjie Wang<sup>1,4</sup>, Edward Emmott<sup>1,5</sup>, Patricia Domingues<sup>1</sup>, Yasmin Chaudhry<sup>1</sup>, Timothy J Fitzmaurice<sup>1</sup>, Matthew K.H. Tung<sup>1</sup>, Marc Panas<sup>6</sup>, Gerald McInerney<sup>6</sup>, Nicholas Locker<sup>7</sup>, Craig B. Willen<sup>8#</sup> and Ian Goodfellow<sup>1#</sup>

1. Division of Virology, Department of Pathology, University of Cambridge
2. Washington University School of Medicine, Department of Pathology and Immunology, St. Louis, MO 63110
3. Department of Microbiology, Harvard Medical School, Boston, MA 02115
4. Institute for Brain Research and Rehabilitation, South China Normal University, Guangzhou 510631, China
5. Department of Bioengineering & Barnett Institute for Chemical and Biological Analyses, Northeastern University, Boston, MA 02115
6. Department of Microbiology, Tumor and Cell Biology, Karolinska Institute, Stockholm, Sweden
7. School of Biosciences and Medicine, University of Surrey, Guildford UK.
8. Yale School of Medicine, Departments of Laboratory Medicine and Immunobiology, New Haven, CT 06520

\* These authors contributed equally to the work

# Corresponding authors:

Craig B Willen: [craig.wilen@yale.edu](mailto:craig.wilen@yale.edu)

Ian Goodfellow: [ig299@cam.ac.uk](mailto:ig299@cam.ac.uk)

1 **Abstract (148)**

2 Knowledge of the host factors required for norovirus replication has been hindered  
3 by the challenges associated with culturing human noroviruses. We have combined  
4 proteomic analysis of the viral translation and replication complexes with a CRISPR  
5 screen, to identify host factors required for norovirus infection. The core stress  
6 granule component G3BP1 was identified as a host factor essential for efficient  
7 human and murine norovirus infection, demonstrating a conserved function across  
8 the *Norovirus* genus. Furthermore, we show that G3BP1 functions in the novel  
9 paradigm of viral VPg-dependent translation initiation, contributing to the assembly of  
10 translation complexes on the VPg-linked viral positive sense RNA genome by  
11 facilitating 40S recruitment. Our data suggest that G3BP1 functions by providing viral  
12 RNA a competitive advantage over capped cellular RNAs, uncovering a novel  
13 function for G3BP1 in the life cycle of positive sense RNA viruses and identifying the  
14 first host factor with pan-norovirus pro-viral activity.

15

16

17 **Keywords (10)**

18

19

20 **Introduction:**

21 Positive sense RNA viruses rely heavily on host cell factors for all aspects of their life  
22 cycle. They replicate on host derived membranous vesicles that are induced  
23 following viral infection, the formation of which requires the activity of key membrane  
24 bound viral enzymes (Altan-Bonnet, 2017). Within the membrane bound viral  
25 replication complex, translation of the viral genome and the synthesis of new viral  
26 RNA occurs in a highly coordinated process. Positive sense RNA viruses have  
27 evolved novel gene expression mechanisms that enable them to overcome the  
28 genome size limitations that accompany error-prone replication and which might  
29 restrict their overall coding capacity (Firth and Brierley, 2012). In addition, viral  
30 modification of the host cell translation machinery often provides a competitive  
31 advantage allowing for the efficient translation of viral RNA in an environment where  
32 competing cellular RNAs are in abundance (McCormick and Khapersky, 2017).  
33 This ability to compete with cellular RNAs is particularly important for the initiation of  
34 infection where the incoming viral genome may be present at only a single copy per  
35 cell.

36 We have previously described a novel paradigm of viral translation that relies on the  
37 interaction of host translation initiation factors with a virus-encoded protein (VPg),  
38 covalently linked to the 5' end of the genome of members of the *Caliciviridae* family  
39 of positive sense RNA viruses (Chaudhry et al., 2006; Chung et al., 2014;  
40 Goodfellow et al., 2005; Hosmillo et al., 2014; Leen et al., 2016). Unlike the 22-  
41 amino acid VPg peptides from picornaviruses, the VPg protein linked to the genomes  
42 of caliciviruses is significantly larger and is essential for the translation of viral RNA  
43 and viral RNA infectivity (Goodfellow, 2011).

44

45 Human noroviruses (HuNoV) and sapoviruses (HuSaV) are enteropathogenic  
46 members of the *Caliciviridae* family of positive sense RNA viruses, and together  
47 cause >20% of all cases of gastroenteritis (GE). They are also a significant cause of  
48 morbidity and mortality in the immunocompromised; individuals with genetic immune-  
49 deficiencies, cancer patients undergoing treatment and transplant recipients often  
50 experience chronic norovirus infections lasting months to years (van Beek et al.,  
51 2016). The economic impact of HuNoV is estimated to be at least ~\$4.2 billion in  
52 direct health care costs, with wider societal costs of ~\$60 billion (Bartsch et al.,  
53 2016). Despite their socioeconomic impact, we have, until very recently lacked a  
54 detailed understanding of much of the norovirus life cycle and many significant  
55 questions remain unanswered. HuNoV replicons (Chang et al., 2006), a murine  
56 norovirus that replicates in cell culture (Karst et al., 2003; Wobus et al., 2004) and  
57 the recent B cell (Jones et al., 2014), stem-cell derived organoid (Ettayebi et al.,  
58 2016) and zebrafish larvae infection models (Van et al., 2019), have all provided  
59 invaluable tools to dissect the norovirus life cycle. However, due to the technical  
60 limitations associated with many of these experimental systems, in comparison to  
61 other positive sense RNA viruses, our knowledge of the intracellular life of  
62 noroviruses is significantly lacking (reviewed in Thorne and Goodfellow, 2014).

63 In the current study, we have combined three independent unbiased approaches to  
64 identify host factors involved in the norovirus life cycle. Combining experimental  
65 systems that incorporated both murine and human noroviruses, allowed the  
66 identification of cellular factors for which the function is likely conserved across the  
67 *Norovirus* genus. By combining three complimentary approaches, we identify the



68 host protein G3BP1 as a critical host factor required for norovirus VPg-dependent  
69 translation, identifying a new role for G3BP1 in virus-specific translation.

## 70 **Results:**

### 71 **Comparative analysis of the norovirus translation initiation complex.**

72 The MNV and the prototype HuNoV Norwalk virus (NV) VPg proteins contain a  
73 highly conserved C-terminal domain (Fig 1A) which we have previously shown to be  
74 necessary and sufficient for binding to the translation initiation factor eIF4G (Chung  
75 et al., 2014; Leen et al., 2016). Using affinity purification on m7-GTP sepharose, we  
76 confirmed that the NV VPg protein, as produced during authentic virus replication in  
77 a NV replicon bearing cell line, interacts with the cap-binding complex eIF4F (Fig  
78 1B). Components of the eIF4F complex, namely the eIF4E cap-binding protein, the  
79 eIF4A helicase and the eIF4GI scaffold protein, along with poly-A binding protein  
80 (PABP) and eIF3 subunits, were readily purified on m7-GTP sepharose, whereas  
81 GAPDH was not. In NV-replicon containing cells, mature VPg was also enriched on  
82 m7-GTP sepharose but the NS3 protein, known to have RNA binding and helicase  
83 activity (Li et al., 2018), was not. Furthermore, we demonstrated that transfection of  
84 GFP-tagged versions of either the MNV or NV VPg proteins into 293T cells allowed  
85 for the affinity purification of eIF4F components and that mutations in the eIF4G  
86 binding domain of VPg reduced this association (Fig 1C).

87

88 We next used quantitative mass spectrometry of the affinity purified complexes  
89 isolated from cells transfected with the GFP-Tagged VPg proteins to identify host  
90 factors specifically enriched on the norovirus VPg protein (Fig 1D, Fig S1 and Table

91 S1). Most of the proteins identified were components of the host cell translation  
92 complex including ribosomal proteins, translation initiation factors and host RNA  
93 binding proteins. These data agrees with but significantly extend our previous  
94 observations using a less sensitive multi-step affinity purification approach to  
95 characterise host factors associated with the MNV VPg protein only (Chaudhry et al.,  
96 2006; Chung et al., 2014). In addition, we identified hnRNPA1 which we have  
97 previously shown to act in norovirus genome circularization (López-Manríquez et al.,  
98 2013). YBX1, DDX3 and several other proteins that we have previously found to  
99 interact with the 5' end of the viral RNA (Vashist et al., 2012b) were also enriched on  
100 VPg (Fig S1). To validate a select number of these interactions and to assess  
101 whether the interaction of VPg with eIF4G is required for their association with VPg,  
102 we performed western blot analysis of complexes purified from cells transfected with  
103 either the WT or eIF4G-binding mutants (Fig 1E). Except for YBX1, the association  
104 of all proteins tested were reduced by the introduction of eIF4G-binding site  
105 mutations into the MNV VPg protein. Together, these data extend our previous  
106 observations and confirm that the norovirus VPg proteins interact with a complex  
107 network of host factors, many of which have been implicated in the host cell  
108 translation initiation process.

109

#### 110 **Determination of the norovirus replication complex proteome.**

111 To further identify the components of the norovirus translation and replication  
112 complex, as formed during authentic viral replication in highly permissive cells, we  
113 utilised two recombinant infectious MNV strains that carried epitope purification tags  
114 within the NS1/2 or NS4 proteins (McCune et al., 2017) (Fig 2A). The insertion

115 positions were previously identified using a transposon based mutagenesis screen  
116 as sites that tolerate insertions, without compromising virus viability (Thorne et al.,  
117 2012). Our approach was somewhat analogous to that recently published for  
118 coronaviruses (V'kovski et al., 2019) but instead used stable isotope labelling of  
119 permissive cells and the FLAG affinity purification tag rather than proximity labelling.  
120 Unlabelled or stable isotope labelled highly permissive BV-2 microglial cells were  
121 infected with either wild type MNV or the equivalent virus carrying the FLAG epitope  
122 purification tag in either NS1/2 or NS4, and the viral replication complex was purified.  
123 The experiment was performed three times by swapping the labelled derivatives of  
124 arginine and lysine as described in the materials and methods. Silver stain of the  
125 purified complexes confirmed the presence of the bait proteins, with both the  
126 uncleaved and cleaved forms of NS1/2 and NS2 being highly enriched (Fig 2B). As  
127 expected, complexes purified from NS1/2-Flag virus infected cells co-purified  
128 untagged NS4 and vice versa (Fig 2B), as we have previously shown these proteins  
129 to interact to form a complex (Thorne et al., 2012). Western blot analysis of the  
130 purified complexes confirmed that viral non-structural and structural proteins were  
131 specifically enriched in the purified complexes, including NS5 (VPg)-containing  
132 precursors (Fig 2C). We noted that anti-NS4 monoclonal antibody was unable to  
133 detect protein in the extracts prior to enrichment, which most likely reflected the  
134 limited sensitivity of the antibody. Quantitative mass spectrometry of the purified  
135 complexes allowed the identified of viral and cellular proteins enriched in the  
136 complex (Fig 2D and Table S2).

137 As expected, all viral proteins, including the VF1 protein product of ORF4, an innate  
138 immune antagonist (Bailey et al., 2011), were enriched in the viral replication  
139 complex. There was a significant correlation between the relative enrichment of

140 proteins identified using NS1/2 and NS4 (Spearman correlation of 0.8832), fitting  
141 with our prior knowledge that both proteins form a complex during viral replication  
142 (Thorne et al., 2012). Ontology analysis indicated that proteins involved in vesicle  
143 transport and fatty acid metabolism were significantly enriched (Fig S2 and Table  
144 S3), fitting with previous observations that the viral replication complex is associated  
145 with cytoplasmic membranous structures (Cotton et al., 2017; Hyde and Mackenzie,  
146 2010; Hyde et al., 2009). Several host proteins previously identified in a variety of  
147 biochemical and genetic screens were enriched (Fig S2 and Table S3) providing  
148 additional confidence that the approach identified biologically relevant interactions.  
149 We noted that the VapA and the paralogue VapB, which we have recently identified  
150 as binding to the NS1/2 protein (McCune et al., 2017), were both highly enriched.  
151 Comparison with the data obtained using VPg as a bait protein (Fig 1) showed some  
152 degree of overlap, however it is worth noting that most of the factors that were  
153 identified using VPg were enriched by >2 fold using only the NS1/2 tagged virus and  
154 not the NS4 tagged virus (Fig S2). One of the exceptions to this was the core stress  
155 granule protein G3BP1, which was enriched by both MNV and NV VPg proteins, and  
156 was also enriched in complexes purified using both NS1/2 and NS4-tagged viruses.

157

158 **Identification of host factors required for norovirus infection using a CRISPR-**  
159 **knockout screen.**

160 A high density CRISPR library screen was undertaken to identify genes that  
161 contribute to the norovirus life cycle. The Brie library (Doench et al., 2016) was  
162 selected due to the reduced off-target effects relative to previously described  
163 CRISPR libraries used for norovirus studies (Haga et al., 2016; Orchard et al., 2016).

164 In addition, to minimise the impact of gRNAs that may have deleterious effects on  
165 long term cell viability and to increase our ability to detect genes that may be  
166 important, but not essential, for norovirus-induced cell death, the infection was  
167 reduced to 24 hours as compared to 2-10 days post infection in previous studies.  
168 BV-2-Cas9 expressing cells were infected with lentiviruses carrying the Brie gRNA  
169 library carrying 78,637 independent guide RNAs to 19,674 genes (Doench et al.,  
170 2016). The transduced cells were then infected with two MNV strains, CW3 and  
171 CR6, which cause acute and persistent infections in immunocompetent mice  
172 respectively (Nice et al., 2012; Thackray et al., 2007), and guide RNA abundance  
173 compared to mock infected cells at 24 hours post infection as illustrated in Fig 3A.  
174 Genes that were enriched by STARS analysis following MNV infection represent  
175 putative pro-viral factors which when disrupted result in slower cell death, whereas  
176 those with a negative STARS value represent putative anti-viral factors where virus-  
177 induced cell death has occurred quicker, resulting in their underrepresentation in the  
178 final pool of cells. MNV-CR6 infection resulted in 212 genes being enriched and 43  
179 being negatively selected (Fig 3B), whereas for MNV-CW3 279 and 19 genes were  
180 positively and negatively selected respectively (Fig 3B). In most cases, there was a  
181 clear correlation between the datasets obtained using either strain (Fig 3C). STARS  
182 analysis was used to rank genes with positive and negative values (Table S4). In  
183 both screens, the MNV receptor Cd300lf was the most highly positively selected  
184 gene identified, in agreement with previous reports (Haga et al., 2016; Orchard et al.,  
185 2016). The second most highly enriched gene was G3BP1, a gene also identified in  
186 one of the two previous CRISPR screens performed on norovirus infected cells  
187 (Orchard et al., 2016).

188

189 A comparison of the data obtained from all three approaches allowed us to identify  
190 several host proteins that were common to all screens (Table S5). G3BP1, the core  
191 stress granule component was identified in all three screens as a potential host  
192 factor essential for norovirus infection. G3BP1 was found to be associated with the  
193 MNV and NV VPg proteins (Fig 1D), enriched in viral replication complexes purified  
194 using either NS1/2 or NS4 flag tagged viruses (Fig 2D) and identified in a CRISPR  
195 screen using two different MNV strains as a putative pro-viral factor involved in the  
196 norovirus life cycle (Fig 3C).

197

#### 198 **G3BP1 is essential for murine norovirus replication**

199 To validate the importance of G3BP1 in the norovirus life cycle we generated G3BP1  
200 deficient BV-2 cell lines (Fig 4A) and examined the impact of G3BP1 ablation on  
201 MNV infection. Western blotting confirmed the loss of G3BP1 in the three lines  
202 tested and we noted that at in some cases, a concomitant increase in G3BP2  
203 expression was observed as has been previously noted (Kedersha et al., 2016). A  
204 clear defect was observed in the ability to replicate to produce infectious virus in  
205 three independently selected  $\Delta$ G3BP1 cell lines (Fig 4B). This effect was mirrored by  
206 an inability to induce cytopathic effect leading to virus-induced cell death (Fig 4C). In  
207 contrast, the ability of encephalomyocarditis virus (EMCV) to infect and cause cell  
208 death was unaffected by the deletion of G3BP1(Fig 4C). These data confirm that  
209 cells lacking G3BP1 are highly resistant to norovirus infection.

210

#### 211 **G3BP1 is essential for human norovirus replication in cell culture**

212 To determine if the G3BP1 was also essential for HuNoV, we examined the impact  
213 of loss of G3BP1 on human norovirus replication in cell culture using the Norwalk  
214 virus replicon. To establish the experimental system, we first confirmed that the  
215 presence of VPg on the 5' end of the Norwalk RNA was essential for the replication  
216 of the replicon RNA and for the capacity to form G418 resistant colonies.  
217 Transfection of replicon RNA, purified from replicon containing cells, into BHK cells  
218 readily resulted in the formation of antibiotic resistant cell colonies (Fig 5A). In  
219 contrast, RNA that was proteinase K treated prior to transfection was unable to  
220 produce replicon containing colonies. Transfection of replicon RNA into wild type  
221 U2OS osteosarcoma cells allowed the formation of replicon-containing colonies,  
222 although the efficiency of formation was significantly less than that seen in BHK cells  
223 (Fig 5B). CRISPR modified U2OS cells that lacked G3BP1 (Kedersha et al., 2016)  
224 were unable to support NV replication, as evident by the lack of antibiotic resistant  
225 colonies (Fig 5B). To further examine the role of G3BP1 in human Norwalk virus  
226 replication, WT or G3BP1 deficient U2OS cells were transfected with NV replicon  
227 VPg-linked RNA, and RNA synthesis monitored overtime following the addition of  
228 G418. While a significant increase in NV viral RNA levels was seen in WT U2OS  
229 cells, those lacking G3BP1 were completely unable to support NV RNA synthesis  
230 (Fig 5C). These data indicate that like for MNV, G3BP1 is essential for human  
231 Norwalk virus replication.

232

233 **The RNA-binding domain of G3BP1 is required for its function in the norovirus**  
234 **life cycle.**

235 To confirm the role of G3BP1 in the norovirus life cycle we examined the ability of full  
236 length and truncated versions of G3BP1 to restore norovirus replication in G3BP1  
237 knockout cells. A mouse BV-2 G3BP1 knockout cell line was complemented with  
238 either full length G3BP1 or variants lacking the RGG or both the RGG and RRM  
239 binding domains (Fig 6A) and the impact on viral replication assessed.  
240 Complementation with full length murine G3BP1 restored the ability of MNV to  
241 induce cell death (Fig 6B) and to produce infectious virus (Fig 6C) back to near wild  
242 type levels. In contrast, complementation with a variant carrying a deletion of the  
243 RGG domain resulted in limited complementation, and deletion of both the RGG and  
244 RRM domains together resulted in complete loss of complementation capacity (Fig  
245 6B&C). These data confirm that the RNA binding domains of G3BP1 are essential  
246 for its function in the norovirus life cycle.

247

#### 248 **G3BP1 is required for a post entry step in the norovirus life cycle.**

249 To further define the role of G3BP1 in the norovirus life cycle we examined whether  
250 G3BP1 functioned at the level of viral entry or post-entry. We therefore bypassed the  
251 entry phase of the infection process and transfected viral VPg-linked RNA into WT  
252 and two independently generated BV-2  $\Delta$ G3BP1 cell lines and examined the impact  
253 on norovirus replication. Transfection of MNV viral VPg-linked RNA into WT cells  
254 resulted in high yields of infectious virus (Fig 7A) and viral proteins (Fig 7C). The  
255 levels of infectivity obtained following transfection of  $\Delta$ G3BP1 cell lines with MNV  
256 viral RNA was comparable to that obtained in WT cells in the presence of the  
257 nucleoside analogue 2'-C-methylcytidin (2CMC), a known inhibitor of the norovirus  
258 RNA polymerase (Rocha-Pereira et al., 2012; 2013) (Fig 7A). No viral proteins were



259 detected in either of the  $\Delta$ G3BP1 cell lines suggesting a defect at a very early stage  
260 in the viral life cycle (Fig 7C). Transfection of VPg-linked RNA into the  $\Delta$ G3BP1 cell  
261 lines reconstituted with WT G3BP1 restored the ability to produce infectious virus  
262 (Fig 7B) and the production of viral proteins (Fig 7D). A minor increase in viral  
263 infectivity was observed in the  $\Delta$ G3BP1 cell line reconstituted with the  $\Delta$ RGG  
264 construct producing viral titres that were higher than those obtained from the WT  
265 complemented line in the presence of 2CMC, suggesting low levels of viral  
266 replication (Fig 7B). However, the levels of viral proteins produced in this line was  
267 below the limit of detection by western blot (Fig 7D). These data confirm that G3BP1  
268 is required for a post entry stage of the norovirus life cycle and that in the absence of  
269 G3BP1 only residual norovirus replication is observed.

270

### 271 **G3BP1 is required for viral negative sense RNA synthesis**

272 To define the precise role of G3BP1 in the early stages of the virus life cycle, we  
273 used strand-specific RT-qPCR to quantify the levels of viral positive and negative  
274 sense RNA in WT and  $\Delta$ G3BP1 cell lines following infection with MNV. As a control,  
275 2CMC was included following virus inoculation as illustrated in the experimental time  
276 line (Fig 8A). The production of viral positive sense RNA was reduced to background  
277 levels in the absence of G3BP1, comparable to levels observed when the 2CMC was  
278 present during the infection (Fig 8B). Viral negative sense RNA synthesis was also  
279 reduced to below the detection limit of the assay in  $\Delta$ G3BP1 cell lines (Fig 8C).  
280 Surprisingly, we were able to detect an ~5 fold increase in viral negative sense RNA  
281 production at 6 hours post infection of WT cells in the presence of 2CMC, which,

282 given that 2CMC was added after the inoculation phase (Fig 8B), likely represents  
283 the first round of viral negative sense RNA synthesis, confirming the sensitivity of the  
284 assay. Addition of 2CMC during the inoculation phase reduced this background  
285 levels (data not shown).

286 Similar results were obtained following transfection of viral RNA into cells to bypass  
287 the entry phase; viral positive and negative sense RNA synthesis was near (or  
288 below) the sensitivity of the assay following transfection of viral VPg-linked RNA into  
289 two independent  $\Delta$ G3BP1 cell lines (Fig 8D & E). Complementation with WT G3BP1,  
290 but not the mutant forms lacking the RNA binding domains, also restored viral  
291 positive and negative sense RNA synthesis (Fig 8F & G). We did not detect viral  
292 positive or negative sense RNAs in the  $\Delta$ RGG complemented cell line, despite the  
293 presence of low levels of viral infectivity (Fig 7B). This discrepancy likely reflects the  
294 relative sensitivities of the assays and the nature of the strand specific qPCR assay  
295 which requires low levels of RNA input to maintain strand specificity. Together these  
296 data suggest that the function of G3BP1 is prior to, or at the level of viral negative  
297 sense RNA synthesis, with the most logical steps being either viral RNA translation  
298 or the formation of viral replication complexes.

299

### 300 **G3BP1 is required for the association of VPg with 40S ribosomal subunits.**

301 We have previously shown that norovirus VPg interacts with eIF4G to recruit  
302 ribosomal subunits and direct viral translation (Chaudhry et al., 2006; Chung et al.,  
303 2014). The interaction between VPg and eIF4G occurs via a direct interaction  
304 between the highly conserved C-terminal region in VPg and the central HEAT

305 domain of eIF4G (Leen et al., 2016) and does not require any additional cellular  
306 cofactors, at least *in vitro*. The interaction between the eIF4G HEAT domain and the  
307 eIF3 complex plays a central role in the recruitment of the 40S ribosomal subunit for  
308 translation initiation (Marcotrigiano:2001uq; Kumar et al., 2016; Villa et al., 2013) .  
309 Our proteomics analysis also confirms that the norovirus VPg proteins form a  
310 complex that contains multiple components of the 40S subunit (Fig 1D) and it has  
311 been established previously that G3BP1 associates with 40S subunits (Kedersha et  
312 al., 2016). To assess a potential role for G3BP1 in the formation of VPg-driven  
313 translation complexes in cells, we examined the ability of GFP tagged version of  
314 MNV VPg to pull down 40S subunits in the presence and absence of G3BP1. GFP-  
315 tagged WT MNV VPg was readily able to pull down eIF4G, G3BP1 and RpS6, a  
316 component of the 40S subunit (Fig 9A). However, in the absence of G3BP1, the  
317 ability to pull down RpS6 was lost (Fig 9A). Furthermore, we found that disruption of  
318 the VPg-eIF4G interaction by the introduction of the F123A mutation into the eIF4G  
319 binding domain, also significantly reduced the ability to pull down RpS6 (Fig 9B).  
320 These data suggest that the interaction of VPg with eIF4G is important for complex  
321 formation with ribosomal proteins and that that G3BP1 contributes in some manner  
322 to the formation of this complex.

323

#### 324 **G3BP1 is require for efficient polysome loading of norovirus VPg-linked RNA**

325 To assess the impact of G3BP on the selective translation of viral VPg-linked RNA  
326 following viral infection, we evaluated the impact of loss of G3BP1 on the recruitment  
327 of viral RNA to polysomes under conditions where viral RNA synthesis was inhibited,  
328 namely in the presence of 2CMC. This approach enabled us to assess only the

329 capacity of the incoming parental viral RNA to assemble into translationally active  
330 complexes, a stage often referred to as the “maiden round” of RNA virus genome  
331 translation. To this aim, cells were infected with MNV in the presence of 2CMC and  
332 polysomes profiling on extracts prepared from cells at 4 and 9 hours post infection  
333 performed (Fig 10A). Quantification of the viral RNA levels in cells in the presence of  
334 2CMC confirmed that the absence of G3BP1 has no impact on the overall levels  
335 present at the time points examined (data not shown). We noted that even in the  
336 presence of 2CMC, which inhibits viral RNA synthesis, there was a small but  
337 measurable increase in free 80S ribosomes over time in WT cells but not in cells  
338 lacking G3BP1 (Fig 10A). We have previously found that MNV infection results in  
339 translation shut off and that this effect is at least partially due to the activity of the  
340 NS6 protease (Emmott et al., 2017). The fact we observed 80S accumulation in WT  
341 cells, even in the absence of viral RNA synthesis, but not in cells lacking G3BP1,  
342 indirectly lead us to suspect that translation of viral RNA had occurred in WT cells,  
343 but was much less efficient in cells lacking G3BP1. Further analyses indicated that  
344 while most ribosome-associated norovirus RNA in WT cells was found in polysomes  
345 containing fractions, less viral RNA was found in ribosome-containing fractions (1-12  
346 in Fig 10A & B) in the absence of G3BP1 cells and, in comparison to WT cells, very  
347 little viral RNA was found in fractions containing polysomes (Fig 10B). Extending the  
348 fractionation to include the free RNA and ribonucleoprotein complexes at the top of  
349 each gradient confirmed that in the absence of G3BP1 norovirus RNA is less  
350 efficient at assembling into polysomal fractions, suggesting a defect at the level of  
351 viral protein synthesis (Fig 10C). Together these data support the hypothesis that  
352 G3BP1 functions to promote the translation of norovirus VPg-linked RNA, by  
353 facilitating the association with 40S subunits.

354

355 **G3BP1 is require for efficient norovirus VPg-dependent translation in the**  
356 **presence of cellular capped RNAs.**

357 To further examine a potential role of G3BP1 in norovirus VPg-dependent  
358 translation, cytoplasmic translationally competent extracts were prepared from WT  
359 and  $\Delta$ G3BP1 cell lines and the translation of highly purified viral VPg-linked viral  
360 RNA (Fig S11A&B) examined. Cap-dependent and cricket paralysis virus IRES  
361 (CrPV)-dependent translation were comparable in nuclease treated extracts  
362 prepared from WT and  $\Delta$ G3BP1 cell lines (Fig 11A), whereas norovirus VPg-  
363 dependent translation was reduced (Fig 11B). Quantification of multiple experiments  
364 indicated that translation in nuclease treated extracts was on average reduced by  
365 ~40-50% because of G3BP1 ablation (Fig 11C). A similar reduction in *in vitro*  
366 translation was observed across multiple time points (Fig S11C).

367

368 The ability of VPg-linked norovirus RNA to be translated in the presence of  
369 increasing amounts of total cellular RNAs was then examined to assess the relative  
370 role of G3BP1 under conditions where cellular RNA are present. Total RNA isolated  
371 from uninfected cells was titrated into the nuclease treated extracts and the impact  
372 norovirus VPg-dependent translation examined (Fig 11D). We found that in the  
373 presence of cellular RNAs, the translation of norovirus VPg-linked RNA in extracts  
374 from  $\Delta$ G3BP1 cells is reduced by up to 80% in comparison to extracts from WT cells.  
375 In agreement with our data using polysome profiling, these data suggest that G3BP1  
376 functions to provide a competitive advantage for norovirus VPg-linked RNA under  
377 conditions where cellular RNAs are present.

378

## 379 **Discussion**

380 In this study, we have used a combination of biochemical and genetic approaches to  
381 identify host factors involved in the norovirus life cycle. Our combined approaches  
382 resulted in the identification of the core stress granule component G3BP1 as a host  
383 protein critical for the replication of both murine and human noroviruses in cell  
384 culture. Furthermore, we determined that G3BP1 plays a key role in the processes of  
385 norovirus VPg-dependent protein synthesis, uncovering a new function for G3BP1 in  
386 facilitating RNA virus genome translation.

387 The orthogonal approaches used in the current study provide an unprecedented  
388 insight into the identity of host factors with potential roles in the norovirus life cycle.  
389 The detailed proteomic analysis of the viral replication and translation complexes  
390 formed during MNV infection (Fig 2) resulted in the identification of several host  
391 factors with previously identified roles in the MNV life cycle. We focused our efforts  
392 on G3BP1 as it was identified in all three approaches and was also identified in a  
393 CRISPR screen published during this study (Orchard et al., 2016). Furthermore, we  
394 have previously shown that feline calicivirus (FCV), a relative of noroviruses within  
395 the *Vesivirus* genus, cleaves G3BP1 to inhibit stress granule formation (Humoud et  
396 al., 2016). In contrast, MNV infection does not result in G3BP1 cleavage and instead  
397 forms cytoplasmic foci the composition of which is distinct from canonical stress  
398 granules (Brocard et al., 2018).

399 G3BP1 is one member of a group of G3BP proteins (Ras-GTPase-activating protein  
400 (SH3 domain)-binding proteins), referred to as Rasputin in insects, that possess

401 RNA binding activity and have multiple cellular functions including the regulation of  
402 RNA stability and translation in response to stress. Originally identified as a protein  
403 that interacted with Ras-GTPase activating protein (RasGAP), more than two  
404 decades of research have significantly expanded our knowledge of the  
405 multifunctional role in cellular processes. It is now well accepted that G3BPs play a  
406 role in cancer cell survival, cancer metastasis and invasion, processing of specific  
407 miRNAs and stress granule formation (Reviewed in (Alam and Kennedy, 2019)).  
408 Stress granules are dynamic cytoplasmic ribonucleoprotein complexes that form  
409 rapidly under stress conditions and within which cellular RNAs are stored in stalled  
410 translation complexes (Protter and Parker, 2016). In the context of viral infection,  
411 numerous studies have suggested that many, if not all, viruses must interact in some  
412 manner with stress granules as there is growing evidence that the formation of  
413 cytoplasmic stress granules is part of the antiviral defence mechanism (Reviewed in  
414 (McCormick and Khapersky, 2017)). Some viruses interact with stress granules to  
415 promote viral replication (Cristea et al., 2010; Kim et al., 2016; Panas et al., 2014;  
416 2012) whereas some do so to counteract the inhibitory effect of stress granules on  
417 the translation of viral RNA (Panas et al., 2015; White et al., 2007).

418 Our data suggests that G3BP1 plays a key role in promoting the translation of  
419 norovirus VPg-linked viral RNA. Positive sense RNA viruses have evolved  
420 mechanisms to ensure the efficient translation of their viral genomic RNAs in the  
421 presence of high concentrations of competing cellular RNAs. These mechanisms  
422 include the use of internal ribosome entry site elements (IRES), modified cap-  
423 dependent mechanisms (Firth and Brierley, 2012; Jaafar and Kieft, 2019) and the  
424 ability to target the host cell translation machinery to generate an environment where  
425 viral RNA translation is favoured over cellular capped RNAs (Walsh et al., 2013).

426 G3BP1 is known to associate primarily with free 40S subunits and not 80S  
427 monosomes (Kedersha et al., 2016). Our data supports a hypothesis whereby the  
428 association of G3BP1 with 40S ribosomal subunits provides a selective advantage  
429 for norovirus VPg-dependent translation, thereby uncovering a new function in virus  
430 specific translation. The mechanism by which G3BP1 contributes to this process has  
431 yet to be fully explored but our data supports the hypothesis that G3BP1 directly or  
432 indirectly promotes the recruitment of 40S ribosomal subunits to VPg-driven  
433 translation complexes. The RGG motif of G3BP1 is known to be essential for the  
434 association between G3BP1 and 40S subunits as well as the ability to form stress  
435 granules, whereas data would suggest that the RRM may play a regulatory role  
436 (Kedersha et al., 2016). These domains were also required for the function of G3BP1  
437 in the norovirus life cycle (Fig 6) confirming that the G3BP1 association with 40S is  
438 important for its role in promoting norovirus VPg-dependent translation. Importantly,  
439 RGG domains are known to have many functions (Thandapani et al., 2013) and  
440 therefore in the context of G3BP1 function in the norovirus life cycle, may also  
441 contribute to unknown interactions that promote norovirus translation. Previous work  
442 on alphaviruses have shown that G3BP1 is sequestered by binding to the nsP3  
443 protein (Panas et al., 2012; 2014; 2015). Furthermore, this interaction occurs via an  
444 FGDF motif also found in other viral proteins including the ICP8 protein of herpes  
445 simplex virus (Panas et al., 2015). While the MNV VPg protein has a similar motif  
446 FGDGF (Fig 1A), this motif is not conserved in the GI Norwalk virus VPg protein.  
447 Therefore our data suggest that the interaction of VPg with G3BP1 is not direct,  
448 fitting with our observation that this interaction is reduced by mutations in the eIF4G  
449 binding domain (Fig 1A and Fig 9B.) While our data fit with a primary role for G3BP1  
450 in norovirus translation, we are unable to exclude the possibility that G3BP1 plays



451 other roles in the viral life cycle. Recent studies have confirmed that G3BP1 is  
452 enriched at sites of viral RNA synthesis (Brocard et al., 2018; Fritzlar et al., 2019) so  
453 it is possible that G3BP1 makes multiple contacts between the 40S subunit and viral  
454 RNA genome directly.

455 The technical challenges associated with studying human norovirus replication in cell  
456 culture have limited the experimental approaches we could use to validate the role of  
457 G3BP1 in human norovirus translation. However, our results have clearly  
458 demonstrated that in the absence of G3BP1, human Norwalk virus is unable to  
459 replicate or form replicon-containing colonies. The presence of G3BP1 in the NV  
460 VPg-containing complexes again fits with our hypothesis that G3BP1 plays a role in  
461 promoting viral VPg-dependent protein synthesis.

462 We have previously found that norovirus infection leads to a translation bias whereby  
463 cellular mRNAs induced in response to infection are inefficiently translated (Emmott  
464 et al., 2017). Our data suggested that this modification of host cell translation was at  
465 least partially driven by the ability of the viral NS6 protease to cleave PABP and the  
466 induction of apoptosis which results in cleavage of cellular translation initiation  
467 factors (Emmott et al., 2017). Furthermore, we have more recently shown that the  
468 ability of the protease to cleave PABP and other substrates is controlled by  
469 polyprotein processing and interactions with other viral proteins (Emmott et al.,  
470 2019). Recent work would agree with our observations and confirms that the  
471 translational bias is not driven by phosphorylation of eIF2 $\alpha$  and that activation of  
472 GCN2 leads to the phosphorylation of eIF2 $\alpha$  (Brocard et al., 2018). We note however  
473 that others have suggested that NS3 may contribute to translational shut off (Fritzlar  
474 et al., 2019), with the caveat that this observation was made outside of the context of

475 infected cells and using overexpressed tagged proteins. We suspect that  
476 noroviruses use multiple mechanisms that work co-operatively to enable the control  
477 of host gene expression and the subsequent translation of the cellular mRNAs. The  
478 relative contribution of these processes in any given cell type may also differ  
479 depending on the degree to which the cells can sense and respond to viral infection  
480 through the induction of innate and apoptotic responses.

481 The observation that many of the factors enriched using the VPg protein were only  
482 enriched on complexes purified with NS1/2 tagged infectious MNV, could suggest  
483 that the viral proteins present in the viral translation complex are distinct from those  
484 present in complexes active for viral RNA synthesis. However, we cannot formally  
485 rule out other possible explanations including the possibility that the specific  
486 enrichment of translation factors on NS1/2 occurs because NS1/2 is the first protein  
487 to be translated from ORF1, therefore unprocessed NS1/2 at the N-terminus of the  
488 ORF1 polyprotein being actively translated could function as an anchor, facilitating  
489 the enrichment of ribosomes and the associated factors. In addition, we have  
490 previously seen that VPg-containing precursors may bind the translation initiation  
491 factor eIF4G less well (Leen et al., 2016), which could prevent some VPg (NS5)  
492 containing precursors associating with translation initiation complexes.

493 In conclusion, our data adds significantly to the growing body of literature on the role  
494 of G3BP proteins in the life cycle of viruses and further extends the functional roles  
495 of G3BP1 to include the promotion of viral translation processes. We identify G3BP1  
496 as a host protein that has a critical role in the life cycle of murine and human  
497 noroviruses, identifying the first cellular pro-viral protein with pan-norovirus activity.  
498 Furthermore, given the apparent importance of G3BP1 to an early stage of the

499 norovirus life cycle, this work suggests that targeting G3BP1 may hold future  
500 therapeutic potential.

501

502 **Grants:**

503 CBW was supported by NIH K08 AI128043 and Burroughs Wellcome Fund. MAM  
504 was supported by NIH U19 AI109725. IG is a Wellcome Senior Fellow. This work  
505 was supported by funding from the Wellcome Trust (Refs: 207498/Z/17/Z and  
506 104914/Z/14/Z ) and the Biotechnology and Biological Sciences Research Council  
507 UK (Refs: BB/N001176/1and BB/000943N/1). JBE was supported by a Churchill  
508 Scholarship.

509

510 **Acknowledgments:**

511 The authors would like to thank Skip Virgin (Washington University in St. Louis) for  
512 intellectual input and the provision of reagents and resources. Kate Heesom of the  
513 University of Bristol Proteomics facility for support with the mass spectrometry  
514 analysis and Nerea Irigoyen (University of Cambridge) for help with polysome  
515 profiling.

516

517

518

519

520

521

522

523

524 **Figure Legends**

525

526 **Figure 1. The norovirus VPg proteins interacts with ribosome associated**  
527 **translation initiation factors.** A) Amino acid sequence alignment of the GV murine  
528 norovirus VPg sequences with VPg from representative human noroviruses from GI  
529 Norwalk virus (NV), GII, and GIV. The position of the site of RNA linkage to the  
530 highly conserved tyrosine residue is highlighted in green. The eIF4G binding motif is  
531 boxed and the position of the C-terminal single amino acid change known to interfere  
532 with eIF4G binding highlighted in orange. B) m7-GTP sepharose was used to affinity  
533 purify eIF4F containing complexes from either wild-type BHK cells (BHK) or BHK  
534 cells containing the Norwalk virus (NV) replicon (BHK-NV). Samples of the lysate (L)  
535 or the affinity purified complexes (m7) were separated by SDS-PAGE then analysed  
536 by western blot for the indicate proteins. Molecular mass shown on the left of the  
537 gels represent the positions of molecular weight markers. C) GFP fusion proteins to  
538 either the wild type (WT) or C-terminal eIF4G binding domain mutants of the MNV  
539 and NV VPg proteins (F123A, F137A) were transfected into human 293T cells and  
540 subjected to immunoaffinity purification using anti-GFP. Samples of the input lysates  
541 (Input) and the purified complexes (GFP-IP) were then separated by SDS-PAGE and  
542 analysed by western blot analysis for the indicated proteins. Mock transfected cells  
543 served as a specificity control. The approximate expected molecular mass of each  
544 protein is shown to the left. D) Quantitative proteomics was used as described in the  
545 text to identify host factors that were affinity purified following transfection of GFP-  
546 tagged derivative of either the NV or MNV VPg proteins. Proteins specifically  
547 enriched in comparison to the GFP control are shown. Data visualisation was  
548 performed using Cystoscape (Shannon et al., 2003) . E) Western blot analysis of cell

549 extracts (Input) or immunoprecipitated (GFP IP) complexes isolated from cells  
550 transfected as described in panel C. For clarity, the molecular masses shown in this  
551 panel refer to the expected mass of the protein being examined.

552

553 **Supplementary Figure 1: Host factors binding to the norovirus VPg.**

554 Quantitative proteomics was used as described in the text to identify host factors that  
555 were affinity purified following transfection of GFP-tagged derivative of either the NV  
556 or MNV VPg proteins. Proteins specifically enriched in comparison to the GFP  
557 control are shown in Panels A and B respectively and where protein binding was  
558 reduced . Panel C illustrates the proteins previously found to interact with the 5' or 3'  
559 termini of the MNV genome (Bailey et al., 2010; Vashist et al., 2012b) or to associate  
560 with MNV VPg using tandem affinity purification (Chung et al., 2014). Data  
561 visualisation was performed using Cytoscape (Shannon et al., 2003)

562

563 **Figure 2: Proteomic characterisation of the norovirus replication complex**

564 **using infectious epitope tagged MNV.** A) Schematic representation of NS1/2-

565 FLAG and NS4-FLAG viruses contain insertions of nucleotide sequences encoding

566 the FLAG peptide DYKDDDDK (in yellow) in their coding sequences. The NS1/2-

567 FLAG virus FLAG peptide was inserted between 2 of the 3 caspase-3 cleavage sites

568 present in NS1/2 (underlined). B) BV-2 cells labelled with stable derivatives of

569 arginine and lysine were infected with either wild type MNV (WT) or recombinant

570 epitope-tagged MNV as described in the materials and methods. 12 hours post

571 infection samples were lysed, samples pooled and immunoaffinity purifications

572 performed as described in the text. Samples of the cell lysates (Input) and the affinity

573 purified complexes (IP:Flag) were analysed by SDS-PAGE on a 4-12% gradient gel

574 prior to silver staining. The positions of the NS1/2, NS2 and NS4 proteins is shown.  
575 C) Western blot analysis of lysates purified from cells infected as described in panel  
576 B, for various viral proteins, confirming the specific enrichment of viral replicase  
577 components. Plot showing detailing overlapping proteins identified in pulldowns from  
578 cells infected with FLAG-tagged NS1/2 or NS4 expressing viruses. All MNV proteins  
579 were identified in association with NS1/2 and NS4 (light blue) including the viral  
580 polymerase NS7, demonstrating enrichment of the MNV replication complex.  
581 Proteins previously identified as host factors potentially involved in some aspect of  
582 the norovirus life cycle through various biochemical or genetic screens are shown in  
583 red. Selected highly enriched proteins are highlighted in black. The NS1/2 binding  
584 partner VapA (McCune et al., 2017) and paralog VapB were both enriched by NS1/2  
585 and NS4.

586

587 **Supplementary Figure 2:** Additional analyses of NS1/2 and NS4-associated  
588 proteins. MNV proteins highlighted in light blue, and G31 in gold. A) Gene ontology  
589 analysis of proteins copurifying with NS1/2 or NS4 ( $\text{Log}_2$  SILAC ratio  $>2$  for either  
590 protein). Proteins in selected, mutually exclusive gene ontology categories were  
591 identified using PANTHER overrepresentation analysis and are plotted in different  
592 colors. B) A number of factors previously identified as MNV host factors using  
593 proteomics or CRISPR approaches (Orchard et al., 2016, Chung et al., 2014,  
594 Vashist et al., 2012) copurified in pulldowns of NS1/2 and NS4 (highlighted red). C)  
595 Novel putative MNV host factors highly enriched ( $\text{Log}_2$  SILAC ratio  $>4$  for either  
596 protein) by NS1/2 and NS4 are plotted in black. D) Proteins identified in pulldowns of  
597 NS1/2 and NS4 which were also identified in pulldowns of MNV VPg are plotted in  
598 red. E) Proteins enriched in pulldowns of NS1/2 and NS4 which were also identified

599 using CRISPR screening as MNV host factors are plotted in red (positive host  
600 factors) and yellow (negative host factors), along with G3bp1 in gold.

601

602 **Figure 3: CRISPR screen identifies host genes positively and negatively**  
603 **selected upon MNV infection.** A) Schematic overview of the infection CRISPR  
604 screen workflow. B) Volcano plot identifying candidate genes enriched upon MNV-  
605 CW3 (red) or MNV-CR6 (blue); red or blue labelled genes correspond to the top-ten  
606 positive or negatively selected genes ranked by the STARS algorithm.

607

608 **Figure 4: CRISPR knockout of G3BP1 renders cells non permissive for MNV**  
609 **replication.** A) Western blot analysis of three independent  $\Delta$ G3BP1 clones for  
610 GAPDH, G3BP1 and G3BP2. B) High multiplicity, single cycle growth curve analysis  
611 of the impact of G3BP1 ablation on MNV replication. BV-2  $\Delta$ G3BP1 clone C cells  
612 were infected at a MOI of 10 TCID<sub>50</sub>/cell, samples were collected at the time points  
613 illustrated, the samples then processed and titrated by TCID<sub>50</sub> as described in the  
614 text. The error bars represent standard errors of three biological repeats and the  
615 data are representative of at least three independent experiments. C) Wild type (WT)  
616 or  $\Delta$ G3BP1 clone C BV-2 cells were plated in a 96 well plate and subsequently  
617 infected using a serial dilution of either EMCV or MNV. Cells were fixed in  
618 paraformaldehyde and stained with crystal violet 5 days post infection. D) Light  
619 micrographs of WT or  $\Delta$ G3BP1 cells either mock infected (-) or infected with EMCV  
620 or MNV and visualised 5 days post infection.

621

622 **Figure 5. G3BP1 is required for human Norwalk virus replication in cell culture.**

623 A) Colony formation ability of human norovirus VPg-linked RNA isolated from BHK-

624 NV replicon containing cells is dependent on the presence of VPg. NV VPg-linked  
625 RNA isolated from BHK-NV cells was either mock treated or treated with proteinase  
626 K prior to transfection into BHK cells. Wells were transfected with either 1.5 $\mu$ g or  
627 0.75 $\mu$ g of total RNA isolated from NV replicon containing BHK cells. Following 2  
628 weeks of antibiotic selection with G418, surviving replicon containing colonies were  
629 fixed and stained with crystal violet in paraformaldehyde. B) NV replicon colony  
630 forming assay in WT and G3BP1<sup>-/-</sup> U2OS cells performed as described in panel A,  
631 with the exception that colonies were stained 12 days post transfection. C)  
632 Quantification of NV replication in WT or  $\Delta$ G3BP1 U2OS cells following transfection  
633 of viral VPg-linked RNA. Viral RNA was quantified by RT-qPCR following  
634 transfection and antibiotic selection. The error bars represent the standard error of  
635 three biological repeats and are representative of three independent experiments.

636

637 **Figure 6: MNV replication in BV-2 cells requires the RNA binding activity of**  
638 **G3BP1.** Western blot analysis of wild type BV-2 cells (WT) or a  $\Delta$ G3BP1 cells (clone  
639 1B2) and the respective complemented lines expressing either WT or the various  
640 G3BP1 truncations. Cells were lysed prior to separation by 12% SDS-PAGE. B) WT  
641 or  $\Delta$ G3BP1 cells complemented with the indicated constructs were plated in a 96  
642 well plate then infected with a serial dilution of MNV, before being fixed and stained 5  
643 days post infection as described in the text. C) WT or  $\Delta$ G3BP1 cells complemented  
644 with the indicated constructs were infected with MNV at an MOI of 10 TCID<sub>50</sub> per  
645 cell. After 24 hours the virus yield was determined by TCID<sub>50</sub>. The error bars  
646 represent the standard error of three independent repeats. The data are  
647 representative of at least two independently repeated experiments.

648



649 **Figure 7: Loss of G3BP1 results in a defect following transfection of viral VPg-**  
650 **linked RNA into  $\Delta$ G3BP1 cells.** A) The indicated cell lines were transfected with  
651 MNV viral RNA and harvested at 9 hours post transfection for TCID50 to assess the  
652 virus yield. In some instances, the nucleoside analogue 2CMC was included to  
653 inhibit viral replication. The dotted line indicates the limit of detection (LOD) and the  
654 error bars represent the standard error from three biological repeats. B) Infectious  
655 virus yield from  $\Delta$ G3BP1 and reconstituted cell lines performed as described in panel  
656 A. C) and D) illustrate the accompanying western blots for samples prepared in  
657 panel A and B respectively. Samples were prepared at 24 hours post transfection,  
658 prior to harvesting, separation by SDS-PAGE on a 4-12% gradient gel prior to  
659 western blotting for the indicated proteins.

660

661 **Figure 8: The Lack of G3BP1 results in a failure to produce viral negative**  
662 **sense RNA.** The experimental design is illustrated in A. Wild type or  $\Delta$ G3BP1 (1B2)  
663 cells were infected prior to the addition of the nucleoside analogue 2CMC to prevent  
664 viral RNA synthesis. Samples were harvest at the indicated time post infection and  
665 viral positive (B) and negative sense RNA quantified by stand specific RT-qPCR (C).  
666 Error bars represent standard error of three biological repeats. LOD refers to the limit  
667 of detection of the assay. D) and E) Viral RNA synthesis following transfection of  
668 viral VPg-linked RNA into WT or two  $\Delta$ G3BP1 cell lines. F) and G) Viral RNA  
669 synthesis following transfection of viral VPg-linked RNA into  $\Delta$ G3BP1 (1B2)  
670 complemented with full length G3BP1 or truncated derivatives.

671

672 **Figure 9: G3BP1 is required for the association of VPg with 40S ribosomal**  
673 **subunits.** A) GFP-Trap immunoprecipitation of complexes isolated on with GFP

674 alone or GFP tagged wild type MNV-VPg demonstrating the pull down of eIF4G1,  
675 G3BP1 and 40S subunits (Rps6). BVv2 cells were transfected with the relevant  
676 constructs, lysates prepared and GFP-Trap pull downs performed as detailed in the  
677 text. Samples were separated by SDS-PAGE and western blotted for the proteins as  
678 shown. B) Mutations in the eIF4G binding domain ablate the association of VPg with  
679 G3BP1 and 40S subunits. GFP-Trap pull downs were performed as described in  
680 panel A with the addition of the MNV VPG Fq123A mutation known to reduce the  
681 association with eIF4G.

682

683 **Figure 10: G3BP1 is required for polysome association of viral RNA**  
684 **association.** A) Polysome profiles of the ribosome containing fractions from mock or  
685 MNV infected wild type (WT) or  $\Delta$ G3BP1 (1B2) BV-2 cells at 4 and 9 hours post  
686 infection (moi 3 TCID50/cell). B) Relative viral RNA levels present in ribosome  
687 containing fractions expressed relative to WT infected BV-2 cells. C) Extended  
688 gradient fractionation of WT or  $\Delta$ G3BP1 cells infected with MNV and harvested 9  
689 hours post infection. Viral RNA levels across the gradient are expressed as  
690 described in panel B.

691

692 **Figure 11: G3BP1 is required for efficient norovirus VPg-dependent**  
693 **translation.**

694 Translation competent extracts from  $\Delta$ G3BP1 cells are fully competent for cap-  
695 dependent and CrPV IRES dependent translation (A). B) Translation of MNV VPg-  
696 linked viral RNA is diminished in extracts prepared from  $\Delta$ G3BP1 cells. Translation of  
697 viral RNA in rabbit reticulocyte lysates (RRL) are used as a side by side comparison.  
698 The positions of the viral proteins are indicated (1-5). C) Quantification of protein

699 products and total translation levels across multiple experiments. The error bars  
700 represent the standard error of three independent experiments. D) Norovirus VPg-  
701 dependent translation in extracts from WT or  $\Delta$ G3BP1 cells in the presence of  
702 increasing concentrations of total cellular RNA isolated from uninfected cells.  
703 Translation of viral RNA in rabbit reticulocyte lysates (RRL) are used as a side by  
704 side comparison. E) Quantification of viral proteins produced in panel (D).

705

706 **Supplementary Figure 11:** A) Characterisation of viral VPg-linked RNA. The  
707 sensitivity of purified MNV VPg-linked RNA to various nucleases was compared to *in*  
708 *vitro* transcribed capped MNV gRNA (cap-gRNA) and the MNV1 full length cDNA  
709 construct. RppH was included as a decapping enzyme require for Xrn1-mediated  
710 cleavage of capped RNAs. Following digestion, the samples were analysed on a 1%  
711 native agarose gel. B) In vitro translation of viral VPg linked RNA in rabbit  
712 reticulocyte lysates demonstrated robust translation and the production of a protein  
713 profile indistinguishable from in vitro transcribed capped genomic RNA (cap-g).  
714 Capped sub-genomic (cap-sg) RNA was included to demonstrate the location of the  
715 VP1 and VP2 proteins. C) The translation of MNV VPg-linked RNA in extracts  
716 prepared from  $\Delta$ G3BP1 cells is reduced across multiple time points. *In vitro*  
717 translations prepared in rabbit reticulocyte lysates (RRL) using *in vitro* transcribed  
718 capped genomic RNA (cap-g) or capped sub-genomic (cap-sg), along with viral VPg-  
719 linked RNA, was used as a reference for the expected mass of the viral proteins.

720

721 **Materials and methods.**

722 **Cells.** The murine microglial BV-2 cell line (Blasi et al., 1990) was provided by  
723 Jennifer Pocock (University College London). BV-2 cells were maintained in DMEM  
724 supplemented with 10% FCS (Biosera), 2 mM L-glutamine, 0.075 % sodium  
725 bicarbonate (Gibco) and the antibiotics penicillin and streptomycin. BHK cells  
726 engineered to express T7 RNA polymerase (BSR-T7 cells, obtained from Karl-Klaus  
727 Conzelmann, Ludwig Maximilians University, Munich, Germany) were maintained in  
728 DMEM containing 10 % FCS, penicillin (100 SI units/ml) and streptomycin (100  
729 µg/ml), and 0.5 mg/ml G418.

730

731 **Generation of G3BP1 KO cells.** BV-2 cells were cultured in DMEM containing 10%  
732 FBS and 1% HEPES. G3BP1 knockout BV-2 cells were generated using two  
733 approaches. The clone 1B2 was generated by transiently transfected with Cas9 and  
734 a sgRNA (5TTCCCCGGCCCCGGCTGATGNGG) targeting exon 7 of G3BP1. BV-2  
735 cells were then single cell cloned and G3BP1 was sequenced by Illumina HiSeq. BV-  
736 2 cells are polyploid at the G3BP1 locus as described previously (Orchard et al.,  
737 2016). Clone 1B2 also had three independent deletions at the sgRNA binding site  
738 resulting in deletions of 1, 2, and 5 base pairs respectively. The mutations introduced  
739 into the 1B2 BV-2 cell clone resulted in frame shifts at nucleotide positions 253, 254  
740 and 244 and the absence of detectable G3BP1 protein as measured by western blot.  
741 G3BP1 knockout BV-2 cell clones A, C and F were generated using an independent  
742 approach that relied on first generating a pool of three lentiviruses carrying guide  
743 RNAs TGTGCAACATGTCCGGGGCC, CAAACTCCCGCCCGACCAGC and  
744 TAGTCCCCTGCTGGTCGGGC targeting the first 100bp of the coding sequence,  
745 cloned into pLentiCRISPRv2 (Sanjana et al., 2014). BV-2 cells were then transduced

746 with the pool of 3 lentiviruses, selected by puromycin treatment for 72 hours, prior to  
747 cloning by limiting dilution. Individual clones were then screened by western blot for  
748 the absence of G3BP1.

749

750 **G3BP1 complementation.** Mouse G3BP1 cDNAs were subcloned into pCDH-MCS-  
751 T2A-puro-MSCV lentiviral vector (System Biosciences) by NEBuilder HiFi DNA  
752 assembly (New England Biolabs). Mouse G3BP1 was subcloned from pCM6-G3BP1  
753 (MR207441; Origene). Mouse G3BP1 lentiviral constructs deficient in the C-terminal  
754 RGG domain (mG3BP1 $\Delta$ RGG) and the RGG and RRM domains  
755 (mG3BP1 $\Delta$ RGGRM) were generated by Gibson cloning from the pCMV6-G3BP1  
756 vector. Lentivirus was generated by co-transfecting pCDH-G3BP1-T2A-puro-MSCV  
757 with pCMV-VSV-G and pSPAX2 into 293T cells with Trans-IT LT1 (Mirus  
758 Biosciences) per manufacture instructions. Two days post-transfection, supernatants  
759 were harvested, filtered through a 0.22 micron filter, and stored at -80C. Lentivirus  
760 encoding G3BP1 or an empty control was then used to transduce G3BP1 KO 1B2  
761 BV-2 cells. Two days post-transduction BV-2 cells were selected with puromycin  
762 (2.5ug/ml) for six days.

763

#### 764 **MNV growth curves**

765 To determine the effects of G3BP1 disruption on MNV replication G3BP1 WT, KO, or  
766 complemented cells were plated in each well of a flat bottom 96-well plate and then  
767 infected with either MNV strains CW1, CW3, or CR6 as described in the text.  
768 Infected cells were flash frozen at -80°C at the times post infection indicated in the  
769 text. Viral replication was then assessed by plaque assay or TCID50 in BV-2 cells as  
770 described in the text. In cases where the appearance of virus-induced cytopathic

771 effect was examined, infected monolayers were either visualized by light microscopy  
772 directly or fixed with crystal violet in formalin, prior to washing and imaging.

773

774 **CRISPR screens.** The CRISPR screen was performed similarly to that described  
775 previously (Orchard et al., 2016) with a number of modifications that included the use  
776 of the Brie gRNA library to reduce off target effects (Doench et al., 2016) and shorter  
777 infection times to improve the recovery of gRNAs that may also compromise cell  
778 viability. BV-2 cells stably expressing Cas9 nuclease (Orchard et al., 2016) were  
779 transduced with the Brie library using previously described protocols (Doench et al.,  
780 2016). MNV strains CW3 and CR6 were used to infect BV-2 CRISPR library at MOI  
781 5 pfu/cell and cells were isolated 24 hours post infection and preparation of gDNA  
782 for sequencing as described previously (Orchard et al., 2016). The screen relies on  
783 the premise that guide RNAs targeting genes that are overrepresented following  
784 infection represent genes that when disrupted are protected against infection and  
785 therefore likely represent factors with pro-viral activity. Likewise, genes for which  
786 guide RNA are underrepresented suggest that infection had proceeded faster and  
787 the gene is antiviral. Following sequencing, the data was analyzed by STARS  
788 method as previously described (Doench et al., 2016; Orchard et al., 2016).  
789 Visualization of candidate genes was accomplished using R (RStudio, Inc., Boston,  
790 MA).

791

792 **Maintenance of SILAC cell lines.** Stable isotope labelling of amino acids in cell  
793 culture of BV-2 cells (SILAC, Ong et al., 2002), was carried out in high-glucose  
794 DMEM lacking arginine and lysine (Sigma-Aldrich), supplemented with dialyzed fetal  
795 bovine serum, 1% L-glutamine, 1X nonessential amino acids, 10 mM HEPES, and

796 1X penicillin/streptomycin. SILAC media were supplemented with Light (R0K0),  
797 Medium (R6K4) or Heavy (R10K8) Arginine and Lysine (Cambridge Isotope  
798 Laboratories). BV-2 cells were maintained in SILAC medium for 2 weeks to ensure  
799 complete metabolic labelling of proteins. Labelling of HEK-293T cells was performed  
800 essentially as described for BV-2 cells, with the omission of 10 mM HEPES and 1X  
801 non-essential amino acids from the cell culture media.

802

803 **DNA based recovery of murine norovirus.** Experiments were performed according  
804 to previously published protocols (Chaudhry et al., 2007). Briefly, BSRT7 cells were  
805 infected to an MOI of 0.5-1 PFU/cell with fowlpox virus expressing T7 RNA  
806 polymerase. Cells were then transfected with a plasmid encoding the MNV full length  
807 clone, or a derivative thereof (e.g. pT7 MNV 383FLAG 3'Rz or pT7 MNV 2600FLAG  
808 3'Rz, our FLAG-tagged virus constructs containing FLAG tags in either NS1/2 or  
809 NS4 respectively). MNV was harvested by freeze-thaw at 24h post-transfection.

810

811 To generate higher titre stocks, WT MNV, NS1/2-FLAG MNV, and NS4-FLAG MNV  
812 (Thorne et al., 2012) generated using the DNA based recovery method described  
813 above were passaged once in BV-2 cells. After 80-90% of cells displayed visible  
814 cytopathic effects (CPE) of viral infection, flasks containing infected cells were frozen  
815 at -80°C. Flasks were frozen and thawed twice before cell debris was removed by  
816 centrifugation at 4000 rpm for 10 minutes in a benchtop centrifuge. Viruses were  
817 pelleted by centrifuging over a 30% sucrose cushion at 76,755xg in a SW32ti rotor  
818 for 2 hours at 4°C. Virus pellets were resuspended overnight in PBS to achieve 100-  
819 fold concentration. Concentrated virus was then passed through a 23-gauge blunt

820 needle 15 times, and clarified by centrifugation at maximum speed in a benchtop  
821 microcentrifuge for 10 minutes. Supernatant aliquoted, and titrated prior to use.

822

823 **Infection of SILAC labelled BV-2 cells with FLAG-tagged viruses.** SILAC-  
824 labelled BV-2 cells were infected with WT MNV, NS1/2-FLAG or NS4-FLAG viruses  
825 at an MOI of 10 TCID<sub>50</sub> cell. Infections were performed in triplicate, using different  
826 combinations of SILAC-labeled BV-2 cells each time to control for any impact of the  
827 SILAC labelling. Infected cells were then plated in the appropriate SILAC media. At  
828 10 hours post-infection, cells were harvested by scraping, and pelleted at 500xg for 5  
829 minutes. Cells were then washed 3 times with ice-cold PBS, and were lysed in (0.5%  
830 Nonidet-P40 substitute, 10 mM Tris-HCl pH 7.5, 150 mM NaCl, 0.5 mM EDTA, 2 mM  
831 MgCl). Benzonase nuclease (Sigma-Aldrich) was added to lysis buffer to a  
832 concentration of 5 µl/ml to prevent nonspecific interactions mediated by RNA or  
833 DNA.

834

835 **Transfection of SILAC labelled HEK-293T cells with GFP-tagged VPg.** SILAC-  
836 labelled HEK-293T cells were transfected with pEGFP-C1 (control) or derivatives  
837 thereof containing either human or murine norovirus VPg protein as described in  
838 Emmott & Goodfellow, (2014). GFP fusions of both wild-type protein or mutant VPg  
839 containing a mutation to inhibit initiation factor binding (MNV: F123A, HuNoV:  
840 F137A) were used. Cells were transfected using Lipofectamine 2000 (Life  
841 Technologies) according to the manufacturers protocol, using antibiotic-free SILAC  
842 media in place of Opti-mem. The experiment was performed in triplicate and SILAC  
843 labels switched in one of the replicates.

844



845 **FLAG and GFP-TRAP immunoprecipitation.** FLAG immunoprecipitations were  
846 performed following the manufacturer's protocol (FLAG M2 beads, Sigma Aldrich) as  
847 described (Thorne et al., 2012). In brief, protein concentration in lysates was  
848 normalized using BCA. Lysates were then diluted with 1 volume of wash buffer (10  
849 mM Tris-Cl pH 7.5, 150 mM NaCl, 0.5 mM EDTA). Equal volumes of anti-FLAG  
850 affinity gel were dispensed into either WT infected cell lysates, or lysates of cells  
851 infected with NS1/2-FLAG or NS4-FLAG. Binding was carried out overnight at 4°C  
852 with rotation. After binding, beads were washed 3 times with wash buffer. All liquid  
853 was carefully removed from each tube, before boiling in SDS-PAGE loading buffer  
854 for 10 minutes. GFP-trap immunoprecipitation of GFP-tagged VPg was  
855 accomplished using GFP-trap beads (Chromotek) per the manufacturer's protocol,  
856 as described (Emmott and Goodfellow, 2014). RNase cocktail (Ambion) was also  
857 included in the lysis buffer at a concentration of 5 µl/ml to prevent non-specific  
858 interactions mediated by RNA. In all cases, light, medium, and heavy-labelled  
859 proteins eluted from the beads for each experimental replicate were pooled together  
860 in a ratio of 1:1:1 before submission for mass spectrometry analysis at the University  
861 of Bristol Proteomics Facility.

862

863 **Mass spectrometry analysis.** Mass spectrometry analysis was performed at the  
864 University of Bristol Proteomics Facility. In brief, samples were run into precast SDS-  
865 PAGE gels for 5 minutes, the entire sample cut from the gel as a single band, and  
866 then subjected to in-gel tryptic digestion including reduction and alkylation using a  
867 ProGest automated digestion unit. The resulting peptides were fractionated using a  
868 Dionex Ultimate 3000 nanoHPLC system in line with an LTQ-Orbitrap Velos or  
869 Orbitrap Tribrid Fusion mass spectrometer.

870

871 **Interpretation of SILAC Proteomics data.** Raw data files were processed and  
872 quantified using Maxquant v1.5.5.1 or 1.6.0.16 (Tyanova *et. al.* 2016). The GFP-VPg  
873 experiments were searched against the Uniprot human database (70,550 entries,  
874 downloaded September 19<sup>th</sup> 2016) plus a custom FASTA file containing the wild-type  
875 and mutant VPg sequences. The raw data, search results and FASTA files can be  
876 found as part of PRIDE submission PXD007585 (Reviewer username:  
877 [reviewer75984@ebi.ac.uk](mailto:reviewer75984@ebi.ac.uk), Password: BH2pTctW). The FLAG-virus experiments  
878 were searched against the Uniprot mouse database (Swiss-prot only, 16,966 entries,  
879 downloaded May 19<sup>th</sup> 2018) plus a custom FASTA file containing the various Murine  
880 norovirus proteins. The raw data, search results and FASTA files can be found as  
881 part of PRIDE submission PXD011779 (Reviewer username:  
882 [reviewer49419@ebi.ac.uk](mailto:reviewer49419@ebi.ac.uk), Password: eLYwivNP). Data were searched with default  
883 Maxquant parameters including upto 2 missed tryptic cleavages, oxidation of  
884 methionine and N-terminal acetylation as variable modifications, and  
885 carbamidomethylation of cysteine as a fixed modification. The data were searched  
886 against a reverse database and PSM and Protein FDR were set to 0.01. The  
887 requantify option was not selected.

888

889 GFP-VPg data were analysed as described previously (Emmott and Goodfellow,  
890 2014). FLAG-virus experiments were analysed by computing the pairwise ratios of  
891 samples infected with NS1/2-FLAG or NS4-FLAG relative to WT MNV-infected  
892 controls. Log<sub>2</sub> SILAC ratios for proteins identified in at least 2/3 replicates were  
893 averaged, and ratios for NS1/2-FLAG:WT and NS4-FLAG:WT were plotted for  
894 comparison of host cell proteins by viral replication complex-associated proteins.

895

896 **Assessment of virus-induced cytopathic effect.** BV-2 WT, KO G3BP1 or  
897 respective G3BP1 complemented cells as described in the text, were seeded onto  
898 96 well plates and infected with serial 10-fold dilutions (starting at MOI=10  
899 TCID<sub>50</sub>/cell) of MNV (CW1) or EMCV. At 48h post-infection, cells were fixed in ice-  
900 cold methanol and stained with toluidine blue prior to washing and imaging.

901

902 **Cap-Sepharose purification for eIF4F complex.** Cell lysates were prepared from  
903 BHK parental cells or BHK containing GI Norwalk virus (BHK-NV) replicon cells in  
904 cap-Sepharose lysis buffer (100 mM KCl, 0.1 mM EDTA, 10% glycerol, 2 mM MgCl<sub>2</sub>,  
905 20 mM HEPES, pH 7.6 in KOH) with 1% TX-100, proteinase and phosphatase  
906 inhibitor cocktails (Calbiochem). Cytoplasmic extracts were centrifuged and RNase  
907 treated for 15 min at room temperature. At least 1000 µg of the cell lysates were  
908 incubated with Sepharose beads coupled to 7-methylguanosine (m<sup>7</sup>GTP, Jena  
909 Biosciences). Input cell lysates were collected for western blot analysis while the  
910 remaining were incubated overnight with continuous rotation at 4°C. The eIF4F-  
911 enriched complex was precipitated and washed 2 times with cap-sepharose lysis  
912 buffer. Bound proteins were eluted in 2x reducing SDS-PAGE samples buffer and  
913 resolved by SDS-PAGE prior to western blot.

914

915 **Human Norwalk virus colony formation assay.** Total RNAs extracts from BHK or  
916 BHK-NV replicon-containing cells (Kitano et al., 2018) were pretreated with and  
917 without proteinase K (10 µg/ml) in 10 mM Tris, pH 8.0, 1.0 mM EDTA, 0.1 M NaCl,  
918 and 0.5% SDS. Pretreated RNAs were immediately purified using GenElute RNA  
919 purification columns (Sigma). Serial 10-fold dilutions of mock or proteinase K-treated

920 RNAs were transfected in BHK cells and 24 h post transfection, cells were passaged  
921 and maintained in growth media containing 0.5 mg/ml G418. Colonies began to form  
922 after 5 d and were allowed to grow until 14 d. All plates were harvested at day 14  
923 and well-formed colonies were fixed in 10% formaldehyde and stained with toluidine  
924 blue. A similar protocol was followed to assess colony formation in U2OS cells with  
925 the exception that selections were maintained for up to 12 days post transfection.  
926 Where indicated, cell aliquots from each time point were collected for qRT-PCR  
927 analysis to assess viral RNA synthesis over time.

928

929 **Polyribosome fractionation analysis.** BV2 WT and BV2  $\Delta$ G3BP1 cells were  
930 seeded at a density of  $7.5 \times 10^6$  cells per T-75 flask, and then either mock infected or  
931 infected with MNV1 (CW1) at MOI 3 TCID<sub>50</sub> per cell in the presence of 2-CMC  
932 (400 $\mu$ M) for each set of infection. After 1h, the inoculum was then removed; the cells  
933 were washed and maintained in growth media containing 2-CMC accordingly until  
934 the cells were harvested at 4h and 9h p.i. Prior to harvesting, cells were treated with  
935 cycloheximide (CHX) for 10 mins at 37°C (Sigma-Aldrich; 100  $\mu$ g/ml) and were  
936 rinsed with 5 ml of ice-cold PBS supplemented with CHX 100  $\mu$ g/ml. Polysome lysis  
937 buffer [20 mM Tris-HCl pH 7.5, 150 mM NaCl, 5mM MgCl, 1 mM DTT, 1% Triton X-  
938 100, 100  $\mu$ g/ml cycloheximide, 25 U/ml TURBO DNase (Life Technologies)] was  
939 used to lyse the cells. Lysates were clarified by centrifugation for 20 min at 13,000 *g*  
940 at 4°C. Aliquots of the lysates were collected for BSA assay and qPCR analysis  
941 against MNV1 RNA before proceeding with fractionation. Input lysates were  
942 normalized to total protein concentration and RT-qPCR was used to confirm the  
943 levels of viral RNA in samples were comparable. Lysates were subjected next to 10-  
944 50% sucrose gradient centrifugation for 90 mins SW41Ti rotor at 190,000  $\times$  *g* at 4°C.

945 The gradients were fractionated at 0.5 ml/min and the levels of RNA in each sample  
946 measured using an in line-254 nm spectrophotometer connected to a chart recorder.  
947 RNAs were extracted from each fraction, converted to cDNA and immediately used  
948 for qPCR. The distribution of viral RNA across the gradient was then calculated as  
949 percentage (%) of the viral RNA seen in WT BV-2 cells using the reference gene  
950 (GAPDH) to obtain normalized values across the gradient. Samples were performed  
951 in duplicates on the same qPCR plate, and the observations were robust across  
952 three independent experiments. Data were collected using a ViiA 7 Real-Time PCR  
953 System (Applied Biosystems).

954

955 **Transfection of VPg-linked MNV RNA into BV-2 cells.** VPg-linked RNA purified  
956 from MNV-1 virus particles was transfected in BV-2 cells using NEON™ as  
957 previously described (Yunus et al., 2010). Total cell lysates were harvested at 3 and  
958 9 hours post transfection with RIPA buffer. 10µg total lysates were analysed by 4-  
959 12% SDS-PAGE (Invitrogen) and antibodies against MNV, VPg, G3BP1 and GAPDH  
960 were used for detection using LI-COR® Odyssey® CLx. Virus yield was determined  
961 by TCID<sub>50</sub>. For strand-specific qPCR detection of MNV RNA, total cellular RNA was  
962 extracted using GeneElute Mammalian Total RNA Miniprep kit (Sigma). RT-qPCR  
963 was performed as described previously (Vashist et al., 2012a).

964

965 **Purification of MNV VPg-linked RNA.** BV-2 cells were infected at an MOI=0.01  
966 TCID<sub>50</sub> per cell and harvested after ~30 post infection. Cell debris was removed by  
967 low speed centrifugation for 10 minutes and supernatant loaded onto 5 ml of 30%  
968 sucrose solution in PBS. MNV particles were pelleted using a SW32Ti rotor at  
969 25,000 RPM for 4 hours at 4 °C. Virus was then resuspended in PBS and total RNA

970 extracted from soluble fraction. Where detailed, the authenticity of the viral RNA was  
971 examined by nuclease digestion. 500 ng of viral RNA or plasmid DNA was treated  
972 with DNase I (10U, Roche), Xrnl+RppH (1U Xrnl + 5U RppH, both from NEB) or  
973 RNase cocktail (0.5U RNase A + 20U RNase T1, ThermoFisher) at 37 °C for 10  
974 minutes. Then analysed on 1% agarose gel.

975

976 **Preparation of BV2 S10 cytoplasmic extracts.** Preparation of BV-2 S10 extracts  
977 was based on a previously published protocol (Rakotondrafara and Hentze, 2011;  
978 2006). BV-2 cells were harvested, washed with PBS, and lysed with 1x packed  
979 volume of hypotonic buffer containing 10 mM HEPES pH7.6, 10 mM potassium  
980 acetate, 0.5 mM magnesium acetate, 5 mM DTT, 1x protease inhibitors cocktail  
981 (EDTA-free, Roche). Cells were lysed on ice for 45 minutes, then passed through  
982 25G and 27G needles to achieve >95% lysis. Cell lysates were then centrifuged at  
983 10,000 x g for 10 minutes at 4 °C twice and the supernatant collected. The total  
984 protein concentration was measured by Bradford assay and normalised to 20 mg/ml  
985 before freezing at -80 °C until use. For micrococcal nuclease treatment, S10 extracts  
986 were thawed on ice, 1 mM calcium chloride and 200 unit/ml final concentrations of  
987 micrococcal nuclease (NEB). Cell lysates were incubated at 25 °C for 15 minutes  
988 before adding 3 mM final concentration of EGTA was added.

989

990 ***In vitro* translation of BV2 S10 lysates.** *In vitro* translation assays were set up  
991 based on a previous protocol (Favre and Trepo, 2001). Translation reactions were  
992 set up in 12.5 µl total volume containing 5 µl BV2 S10 lysate, 2.5 µl 5X translation  
993 buffer, 0.25 µl of 5 mg/ml creatine kinase, 1.25 µl RRL, 0.225 µl of 5 M potassium  
994 acetate, 0.25 mM of 100 mM magnesium acetate, 5.13 µCi <sup>35</sup>S-labelled methionine

995 (PerkinElmer) and 10-100 ng/μl RNA as detailed in the text. 5X translation buffer  
996 contains 350 mM HEPES, 75 mM creatine phosphate, 10 mM ATP, 3.75 mM GTP,  
997 100 μM amino acid minus methionine, 3.75 mM spermidine and 0.375 mM S-  
998 adenosyl-methionine. For control experiments using RRL (Promega), the reactions  
999 were set up according to manufacturer's instructions using 0.5-1 ng/μl RNA.  
1000 Reactions were incubated at 30 °C for 90 minutes before addition of 12.5 μl trans-  
1001 stop buffer containing 10 mM EDTA and 0.1 mg/ml RNase A and incubated at room  
1002 temperature for 10 minutes, then 25 μl 5X loading buffer was added to the reaction  
1003 and heated at 95 °C for 5 minutes. 10 μl lysates were resolved in 15% SDS-PAGE  
1004 and exposed to a phosphorimager screen and visualised using a TyphoonFLA7000  
1005 machine. For non-radioactive translation, 1.25 μl of 1 mM methionine was used  
1006 instead of <sup>35</sup>S-labelled methionine, and the reactions were stopped with 100 μl 1x  
1007 passive lysis buffer (Promega) and the luminescence read using a GloMax  
1008 luminometer (Promega).

## References:

Alam, U., and Kennedy, D. (2019). Rasputin a decade on and more promiscuous than ever? A review of G3BPs. *Biochim Biophys Acta Mol Cell Res* 1866, 360–370.

Altan-Bonnet, N. (2017). Lipid Tales of Viral Replication and Transmission. *Trends Cell Biol.* 27, 201–213.

Bailey, D., Carrara, G., Benson, A., Chaudhry, Y., Heeney, J., Yarovinsky, F., Simmonds, P., Goodfellow, I., McFadden, N., Shortland, A., et al. (2011). Norovirus regulation of the innate immune response and apoptosis occurs via the product of the alternative open reading frame 4. *PLoS Pathog.* 7, e1002413.

Bailey, D., Karakasiliotis, I., Vashist, S., Chung, L.M.W., Rees, J., Reese, J., McFadden, N., Benson, A., Yarovinsky, F., Simmonds, P., et al. (2010). Functional analysis of RNA structures present at the 3' extremity of the murine norovirus genome: the variable polypyrimidine tract plays a role in viral virulence. *J Virol* 84, 2859–2870.

Bartsch, S.M., Lopman, B.A., Ozawa, S., Hall, A.J., and Lee, B.Y. (2016). Global Economic Burden of Norovirus Gastroenteritis. *PLoS ONE* 11, e0151219.

Blasi, E., Barluzzi, R., Bocchini, V., Mazzolla, R., and Bistoni, F. (1990). Immortalization of murine microglial cells by a v-raf/v-myc carrying retrovirus. *J. Neuroimmunol.* 27, 229–237.

Brocard, M., Iadevaia, V., Klein, P., Hall, B., Lewis, G., Lu, J., Burke, J., Parker, R., Ruggieri, A., Goodfellow, I., et al. (2018). Norovirus infection results in assembly of virus-specific G3BP1 granules and evasion of eIF2 $\alpha$  signaling. *bioRxiv* 490318.

Chang, K.-O., Sosnovtsev, S.V., Belliot, G., King, A.D., and Green, K.Y. (2006). Stable expression of a Norwalk virus RNA replicon in a human hepatoma cell line. *Virology* 353, 463–473.

Chaudhry, Y., Nayak, A., Bordeleau, M.-E., Tanaka, J., Pelletier, J., Belsham, G.J., Roberts, L.O., and Goodfellow, I.G. (2006). Caliciviruses differ in their functional requirements for eIF4F components. *J. Biol. Chem.* 281, 25315–25325.

Chaudhry, Y., Skinner, M.A., and Goodfellow, I.G. (2007). Recovery of genetically defined murine norovirus in tissue culture by using a fowlpox virus expressing T7 RNA polymerase. *J. Gen. Virol.* 88, 2091–2100.

Chung, L., Bailey, D., Leen, E.N., Emmott, E.P., Chaudhry, Y., Roberts, L.O., Curry, S., Locker, N., and Goodfellow, I.G. (2014). Norovirus translation requires an interaction between the C Terminus of the genome-linked viral protein VPg and eukaryotic translation initiation factor 4G. *J. Biol. Chem.* 289, 21738–21750.

Cotton, B.T., Hyde, J.L., Sarvestani, S.T., Sosnovtsev, S.V., Green, K.Y., White, P.A., and Mackenzie, J.M. (2017). The Norovirus NS3 Protein Is a Dynamic Lipid- and Microtubule-Associated Protein Involved in Viral RNA Replication. *J Virol* 91, e02138–16.



Cristea, I.M., Rozjabek, H., Molloy, K.R., Karki, S., White, L.L., Rice, C.M., Rout, M.P., Chait, B.T., and MacDonald, M.R. (2010). Host factors associated with the Sindbis virus RNA-dependent RNA polymerase: role for G3BP1 and G3BP2 in virus replication. *J Virol* 84, 6720–6732.

Doench, J.G., Fusi, N., Sullender, M., Hegde, M., Vaimberg, E.W., Donovan, K.F., Smith, I., Tothova, Z., Wilen, C., Orchard, R., et al. (2016). Optimized sgRNA design to maximize activity and minimize off-target effects of CRISPR-Cas9. *Nat. Biotechnol.* 34, 184–191.

Emmott, E., and Goodfellow, I. (2014). Identification of protein interaction partners in mammalian cells using SILAC-immunoprecipitation quantitative proteomics. *J Vis Exp* e51656–e51656.

Emmott, E., de Rougemont, A., Hosmillo, M., Lu, J., Fitzmaurice, T.J., Haas, J., and Goodfellow, I. (2019). Polyprotein processing and intermolecular interactions within the viral replication complex spatially and temporally control norovirus protease activity. *J. Biol. Chem.* jbc.RA118.006780.

Emmott, E., Sorgeloos, F., Caddy, S.L., Vashist, S., Sosnovtsev, S., Lloyd, R., Heesom, K., Locker, N., and Goodfellow, I. (2017). Norovirus-mediated modification of the translational landscape via virus and host-induced cleavage of translation initiation factors. *Mol. Cell Proteomics* mcp.M116.062448.

Ettayebi, K., Crawford, S.E., Murakami, K., Broughman, J.R., Karandikar, U., Tenge, V.R., Neill, F.H., Blutt, S.E., Zeng, X.-L., Qu, L., et al. (2016). Replication of human noroviruses in stem cell-derived human enteroids. *Science* 353, 1387–1393.

Favre, D., and Treppe, C. (2001). Translational extracts active biologically in vitro obtained from eukaryotic monolayer cells: a versatile method for viral RNA studies. *J. Virol. Methods* 92, 177–181.

Firth, A.E., and Brierley, I. (2012). Non-canonical translation in RNA viruses. *J. Gen. Virol.* 93, 1385–1409.

Fritzlar, S., Aktepe, T., Chao, Y.-W., McAllaster, M., Wilen, C., White, P., and Mackenzie, J. (2019). Mouse Norovirus infection arrests host cell translation uncoupled from the stress granule-PKR-eIF2 $\alpha$  axis. *bioRxiv* 536052.

Goodfellow, I. (2011). The genome-linked protein VPg of vertebrate viruses — a multifaceted protein. *Curr Opin Virol* 1, 355–362.

Goodfellow, I., Chaudhry, Y., Gioldasi, I., Gerondopoulos, A., Natoni, A., Labrie, L., Laliberté, J.-F., and Roberts, L. (2005). Calicivirus translation initiation requires an interaction between VPg and eIF 4 E. *EMBO Rep.* 6, 968–972.

Haga, K., Fujimoto, A., Takai-Todaka, R., Miki, M., Doan, Y.H., Murakami, K., Yokoyama, M., Murata, K., Nakanishi, A., and Katayama, K. (2016). Functional receptor molecules CD300lf and CD300ld within the CD300 family enable murine noroviruses to infect cells. *Proc. Natl. Acad. Sci. U.S.a.* 113, E6248–E6255.

Hosmillo, M., Chaudhry, Y., Kim, D.-S., Goodfellow, I., and Cho, K.-O. (2014).

Sapovirus translation requires an interaction between VPg and the cap binding protein eIF4E. *J Virol* 88, 12213–12221.

Humoud, M.N., Doyle, N., Royall, E., Willcocks, M.M., Sorgeloos, F., van Kuppeveld, F., Roberts, L.O., Goodfellow, I.G., Langereis, M.A., and Locker, N. (2016). Feline Calicivirus Infection Disrupts Assembly of Cytoplasmic Stress Granules and Induces G3BP1 Cleavage. *J Virol* 90, 6489–6501.

Hyde, J.L., and Mackenzie, J.M. (2010). Subcellular localization of the MNV-1 ORF1 proteins and their potential roles in the formation of the MNV-1 replication complex. *Virology* 406, 138–148.

Hyde, J.L., Sosnovtsev, S.V., Green, K.Y., Wobus, C., Virgin, H.W., and Mackenzie, J.M. (2009). Mouse norovirus replication is associated with virus-induced vesicle clusters originating from membranes derived from the secretory pathway. *J Virol* 83, 9709–9719.

Jaafar, Z.A., and Kieft, J.S. (2019). Viral RNA structure-based strategies to manipulate translation. *Nat. Rev. Microbiol.* 17, 110–123.

Jones, M.K., Watanabe, M., Zhu, S., Graves, C.L., Keyes, L.R., Grau, K.R., Gonzalez-Hernandez, M.B., Iovine, N.M., Wobus, C.E., Vinjé, J., et al. (2014). Enteric bacteria promote human and mouse norovirus infection of B cells. *Science* 346, 755–759.

Karst, S.M., Wobus, C.E., Lay, M., Davidson, J., and Virgin, H.W. (2003). STAT1-dependent innate immunity to a Norwalk-like virus. *Science* 299, 1575–1578.

Kedersha, N., Panas, M.D., Achorn, C.A., Lyons, S., Tisdale, S., Hickman, T., Thomas, M., Lieberman, J., McInerney, G.M., Ivanov, P., et al. (2016). G3BP-Caprin1-USP10 complexes mediate stress granule condensation and associate with 40S subunits. *J. Cell Biol.* 212, 845–860.

Kim, D.Y., Reynaud, J.M., Rasaloukaya, A., Akhrymuk, I., Mobley, J.A., Frolov, I., and Frolova, E.I. (2016). New World and Old World Alphaviruses Have Evolved to Exploit Different Components of Stress Granules, FXR and G3BP Proteins, for Assembly of Viral Replication Complexes. *PLoS Pathog.* 12, e1005810.

Kitano, M., Hosmillo, M., Emmott, E., Lu, J., and Goodfellow, I. (2018). Selection and Characterization of Rupintrivir-Resistant Norwalk Virus Replicon Cells In Vitro. *Antimicrob. Agents Chemother.* 62, 725.

Kumar, P., Hellen, C.U.T., and Pestova, T.V. (2016). Toward the mechanism of eIF4F-mediated ribosomal attachment to mammalian capped mRNAs. *Genes Dev.* 30, 1573–1588.

Leen, E.N., Sorgeloos, F., Correia, S., Chaudhry, Y., Cannac, F., Pastore, C., Xu, Y., Graham, S.C., Matthews, S.J., Goodfellow, I.G., et al. (2016). A Conserved Interaction between a C-Terminal Motif in Norovirus VPg and the HEAT-1 Domain of eIF4G Is Essential for Translation Initiation. *PLoS Pathog.* 12, e1005379.

Li, T.-F., Hosmillo, M., Schwanke, H., Shu, T., Wang, Z., Yin, L., Curry, S.,

Goodfellow, I.G., and Zhou, X. (2018). Human Norovirus NS3 Has RNA Helicase and Chaperoning Activities. *J Virol* 92, 312.

López-Manríquez, E., Vashist, S., Ureña, L., Goodfellow, I., Chavez, P., Mora-Heredia, J.E., Cancio-Lonches, C., Garrido, E., and Gutiérrez-Escolano, A.L. (2013). Norovirus Genome Circularisation and Efficient Replication is Facilitated by Binding of PCBP2 and hnRNP A1. *J Virol* 87, 11371–11387.

McCormick, C., and Khapersky, D.A. (2017). Translation inhibition and stress granules in the antiviral immune response. *Nat. Rev. Immunol.* 17, 647–660.

McCune, B.T., Tang, W., Lu, J., Eaglesham, J.B., Thorne, L., Mayer, A.E., Condiff, E., Nice, T.J., Goodfellow, I., Krezel, A.M., et al. (2017). Noroviruses Co-opt the Function of Host Proteins VAPA and VAPB for Replication via a Phenylalanine-Phenylalanine-Acidic-Tract-Motif Mimic in Nonstructural Viral Protein NS1/2. *MBio* 8, e00668–17.

Nice, T.J., Strong, D.W., McCune, B.T., Pohl, C.S., and Virgin, H.W. (2012). A single amino acid change in murine norovirus NS1/2 is sufficient for colonic tropism and persistence. *J Virol*.

Orchard, R.C., Wilen, C.B., Doench, J.G., Baldrige, M.T., McCune, B.T., Lee, Y.-C.J., Lee, S., Pruett-Miller, S.M., Nelson, C.A., Fremont, D.H., et al. (2016). Discovery of a proteinaceous cellular receptor for a norovirus. *Science* 353, 933–936.

Panas, M.D., Ahola, T., and McInerney, G.M. (2014). The C-terminal repeat domains of nsP3 from the Old World alphaviruses bind directly to G3BP. *J Virol* 88, 5888–5893.

Panas, M.D., Schulte, T., Thaa, B., Sandalova, T., Kedersha, N., Achour, A., and McInerney, G.M. (2015). Viral and cellular proteins containing FGDF motifs bind G3BP to block stress granule formation. *PLoS Pathog.* 11, e1004659.

Panas, M.D., Varjak, M., Lulla, A., Eng, K.E., Merits, A., Karlsson Hedestam, G.B., and McInerney, G.M. (2012). Sequestration of G3BP coupled with efficient translation inhibits stress granules in Semliki Forest virus infection. *Mol Biol Cell* 23, 4701–4712.

Protter, D.S.W., and Parker, R. (2016). Principles and Properties of Stress Granules. *Trends Cell Biol.* 26, 668–679.

Rakotondrafara, A.M., and Hentze, M.W. (2011). An efficient factor-depleted mammalian in vitro translation system. *Nat Protoc* 6, 563–571.

Rocha-Pereira, J., Jochmans, D., Dallmeier, K., Leyssen, P., Cunha, R., Costa, I., Nascimento, M.S.J., and Neyts, J. (2012). Inhibition of norovirus replication by the nucleoside analogue 2'-C-methylcytidine. *Biochem. Biophys. Res. Commun.* 427, 796–800.

Rocha-Pereira, J., Jochmans, D., Debing, Y., Verbeken, E., Nascimento, M.S.J., and Neyts, J. (2013). The viral polymerase inhibitor 2'-C-methylcytidine inhibits Norwalk

virus replication and protects against norovirus-induced diarrhea and mortality in a mouse model. *J Virol* *87*, 11798–11805.

Sanjana, N.E., Shalem, O., and Zhang, F. (2014). Improved vectors and genome-wide libraries for CRISPR screening. *Nat. Methods* *11*, 783–784.

Shannon, P., Markiel, A., Ozier, O., Baliga, N.S., Wang, J.T., Ramage, D., Amin, N., Schwikowski, B., and Ideker, T. (2003). Cytoscape: a software environment for integrated models of biomolecular interaction networks. *Genome Res.* *13*, 2498–2504.

Thackray, L.B., Wobus, C.E., Chachu, K.A., Liu, B., Alegre, E.R., Henderson, K.S., Kelley, S.T., and Virgin, H.W. (2007). Murine noroviruses comprising a single genogroup exhibit biological diversity despite limited sequence divergence. *J Virol* *81*, 10460–10473.

Thandapani, P., O'Connor, T.R., Bailey, T.L., and Richard, S. (2013). Defining the RGG/RG motif. *Mol. Cell* *50*, 613–623.

Thorne, L.G., and Goodfellow, I.G. (2014). Norovirus gene expression and replication. *J. Gen. Virol.* *95*, 278–291.

Thorne, L., Bailey, D., and Goodfellow, I. (2012). High-Resolution functional profiling of the norovirus genome. *J Virol* *86*, 11441–11456.

V'kovski, P., Gerber, M., Kelly, J., Pfaender, S., Ebert, N., Braga Lagache, S., Simillion, C., Portmann, J., Stalder, H., Gaschen, V., et al. (2019). Determination of host proteins composing the microenvironment of coronavirus replicase complexes by proximity-labeling. *Elife* *8*, 25.

van Beek, J., van der Eijk, A.A., Fraaij, P.L.A., Caliskan, K., Cransberg, K., Dalinghaus, M., Hoek, R.A.S., Metselaar, H.J., Roodnat, J., Vennema, H., et al. (2016). Chronic norovirus infection among solid organ recipients in a tertiary care hospital, the Netherlands, 2006-2014. *Clin. Microbiol. Infect.*

Van, J.D., Ny, A., Conceição-Neto, N., Maes, J., Hosmillo, M., Cuvry, A., Goodfellow, I., de, T.A.N., Verbeken, E., Matthijnssens, J., et al. (2019). A robust human norovirus replication model in zebrafish larvae: Supplementary data file. *bioRxiv* 528364.

Vashist, S., Ureña, L., and Goodfellow, I. (2012a). Development of a strand specific real-time RT-qPCR assay for the detection and quantitation of murine norovirus RNA. *J. Virol. Methods.*

Vashist, S., Ureña, L., Chaudhry, Y., and Goodfellow, I. (2012b). Identification of RNA-protein interaction networks involved in the norovirus life cycle. *J Virol* *86*, 11977–11990.

Villa, N., Do, A., Hershey, J.W.B., and Fraser, C.S. (2013). Human Eukaryotic Initiation Factor 4G (eIF4G) Protein Binds to eIF3c, -d, and -e to Promote mRNA Recruitment to the Ribosome. *J. Biol. Chem.* *288*, 32932–32940.

Walsh, D., Mathews, M.B., and Mohr, I. (2013). Tinkering with translation: protein synthesis in virus-infected cells. *Cold Spring Harb Perspect Biol* 5, a012351–a012351.

White, J.P., Cardenas, A.M., Marissen, W.E., and Lloyd, R.E. (2007). Inhibition of cytoplasmic mRNA stress granule formation by a viral proteinase. *Cell Host Microbe* 2, 295–305.

Wobus, C.E., Karst, S.M., Thackray, L.B., Chang, K.-O., Sosnovtsev, S.V., Belliot, G., Krug, A., Mackenzie, J.M., Green, K.Y., and Virgin, H.W. (2004). Replication of Norovirus in cell culture reveals a tropism for dendritic cells and macrophages. *PLoS Biol.* 2, e432.

Yunus, M.A., Chung, L.M.W., Chaudhry, Y., Bailey, D., and Goodfellow, I. (2010). Development of an optimized RNA-based murine norovirus reverse genetics system. *J. Virol. Methods* 169, 112–118.

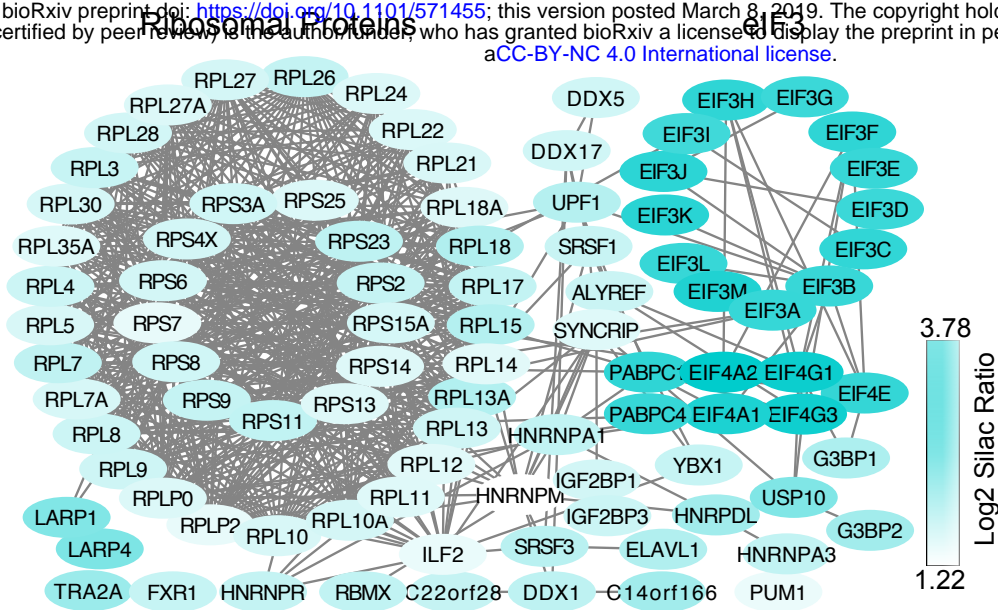
(2006). Differential Cleavage of eIF4GI and eIF4GII in Mammalian Cells. 1–12.



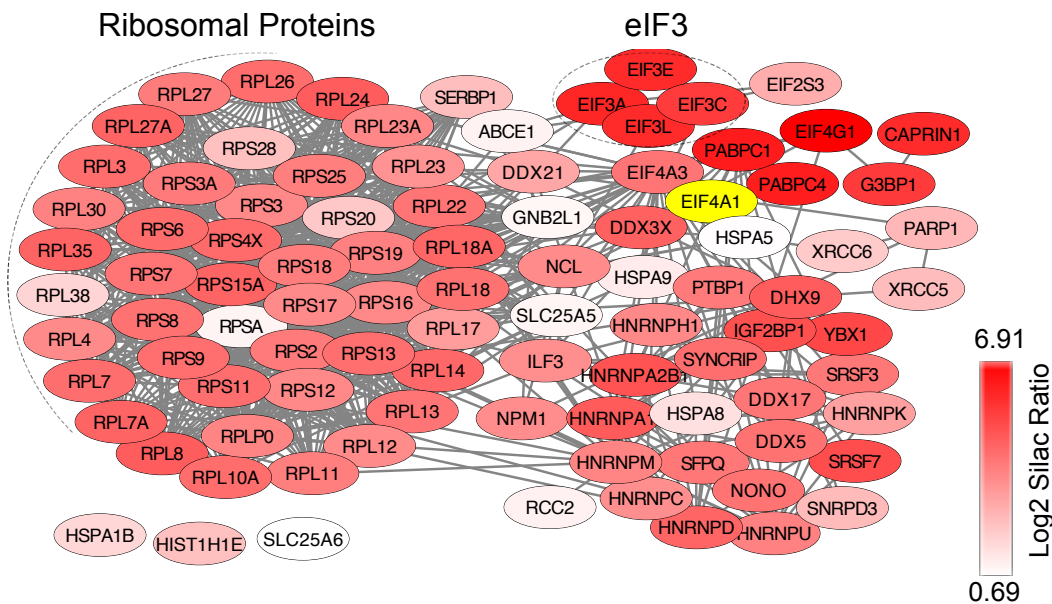


A. Host proteins binding to the murine norovirus VPg protein

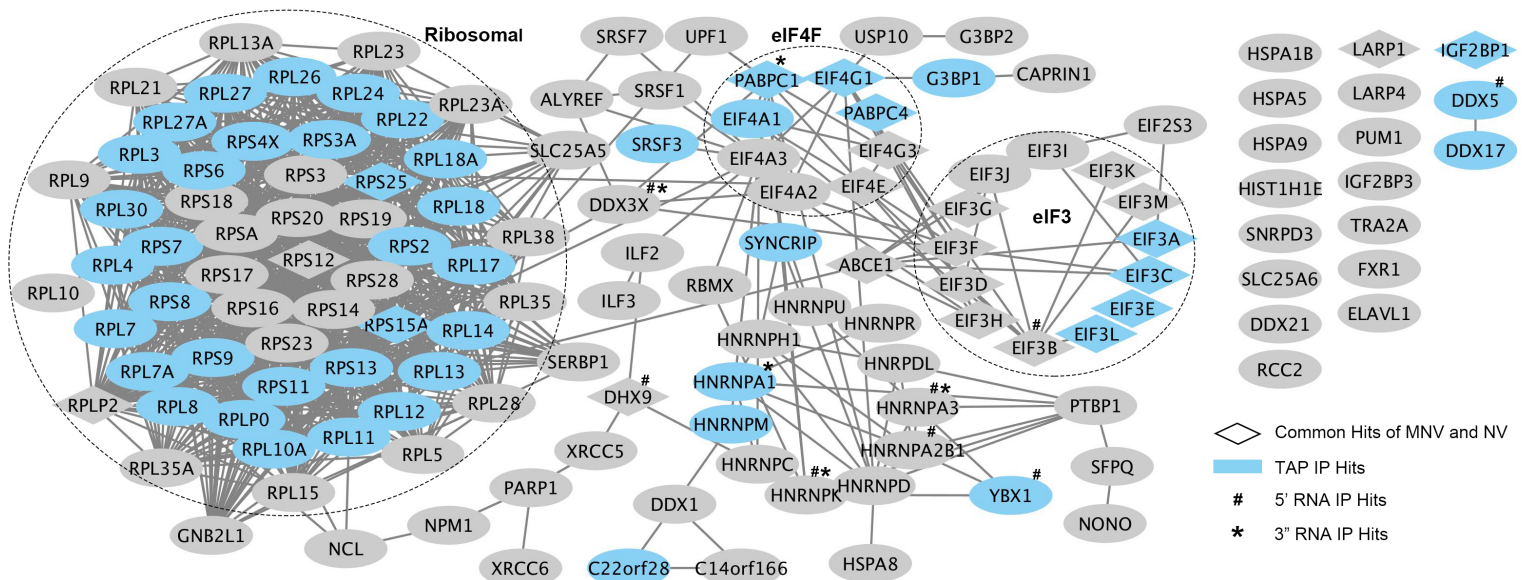
bioRxiv preprint doi: <https://doi.org/10.1101/571455>; this version posted March 8, 2019. The copyright holder for this preprint (which was not certified by peer review) is the author/funder, who has granted bioRxiv a license to display the preprint in perpetuity. It is made available under aCC-BY-NC 4.0 International license.



B. Host proteins binding to the Norwalk virus VPg

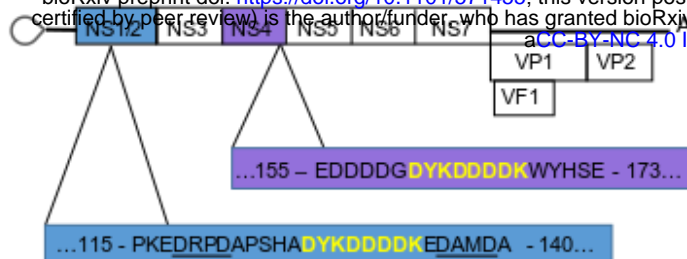
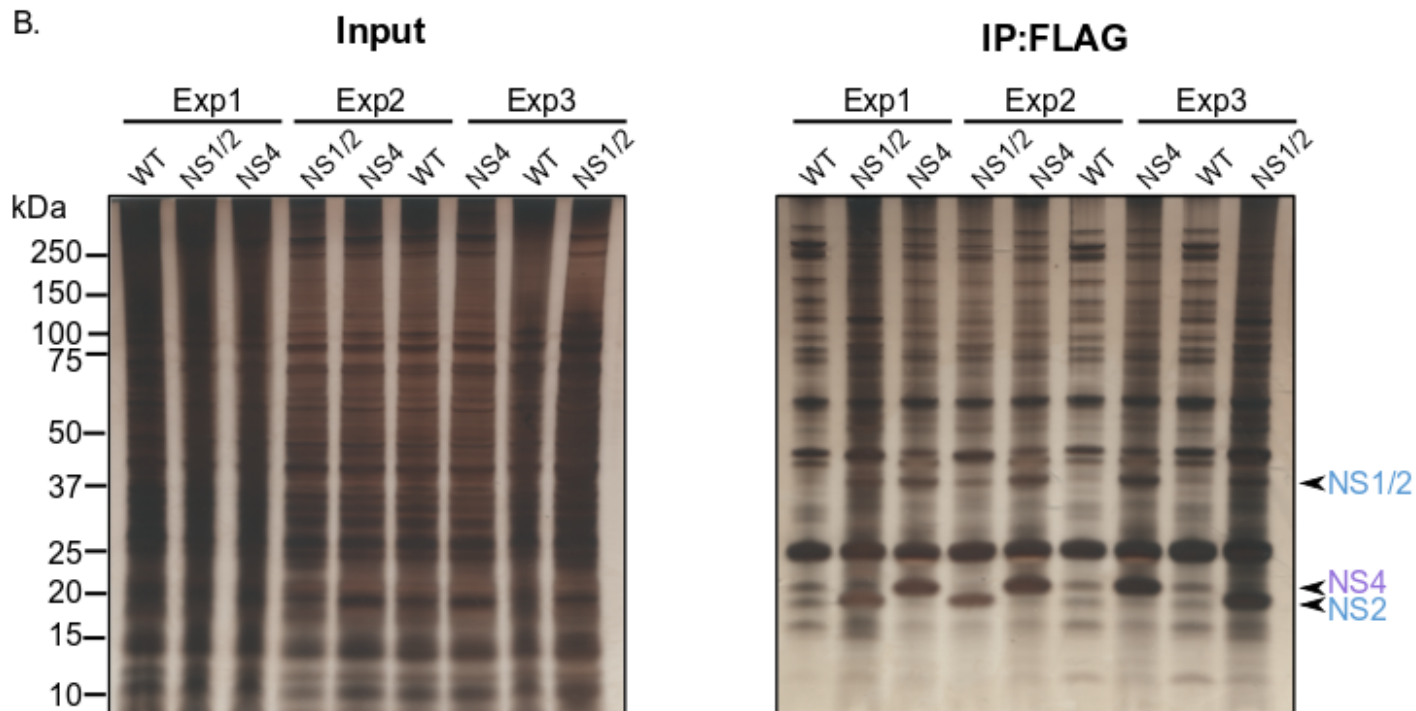
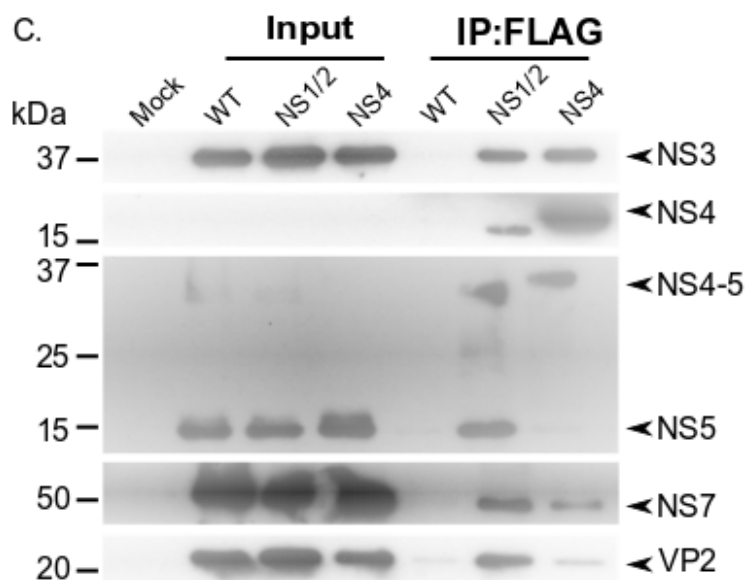
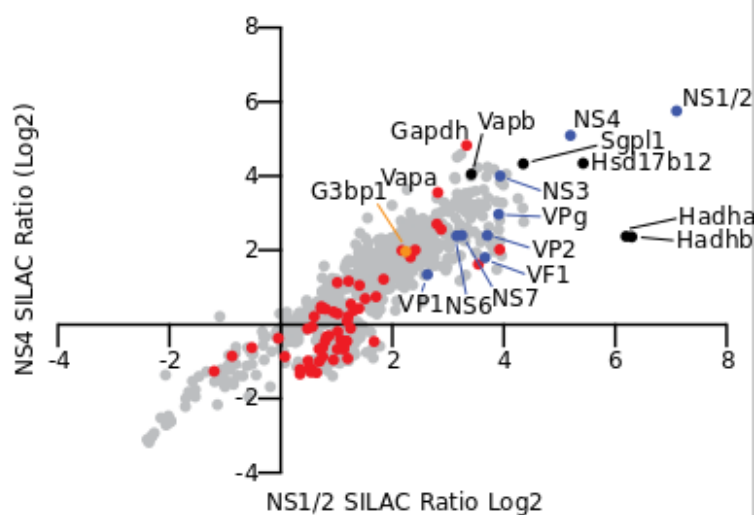


C. Host proteins previously identified as interacting with the MNV VPg protein or the termini of the MNV genomic RNA



**Figure 2****A.**

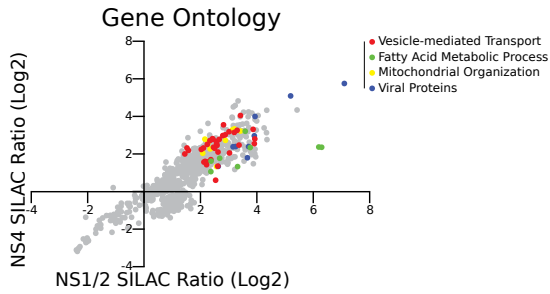
bioRxiv preprint doi: <https://doi.org/10.1101/571455>; this version posted March 8, 2019. The copyright holder for this preprint (which was not certified by peer review) is the author/funder, who has granted bioRxiv a license to display the preprint in perpetuity. It is made available under aCC-BY-NC 4.0 International license.

**B.****C.****D.**

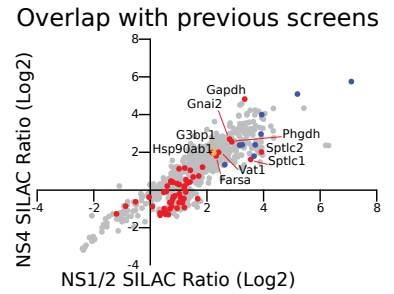


# Supplementary Figure 2

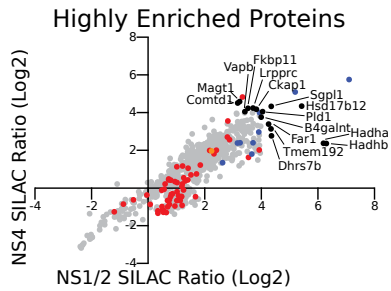
A.



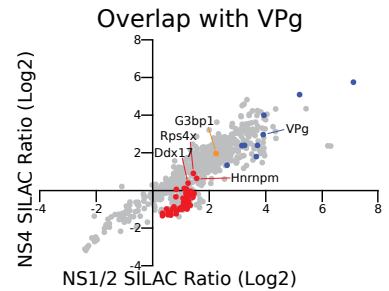
B.



C.



D.



E.

Overlap with Brie CRISPR screen

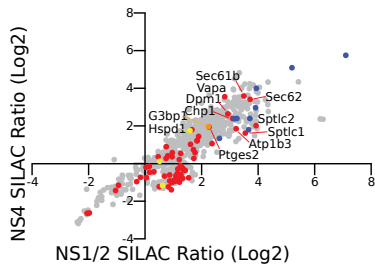


**Figure 3**

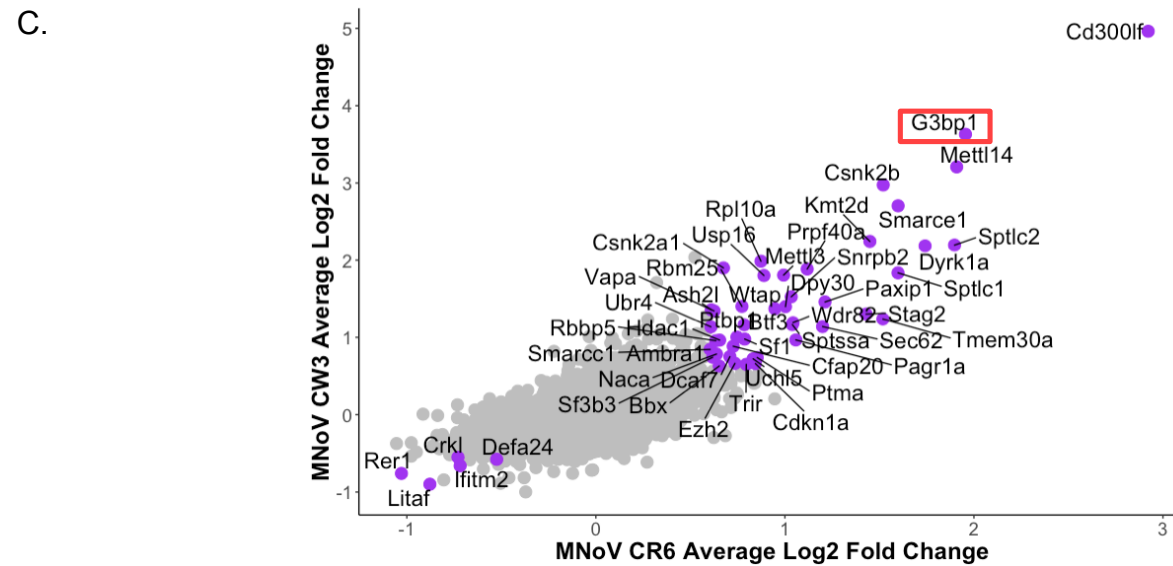
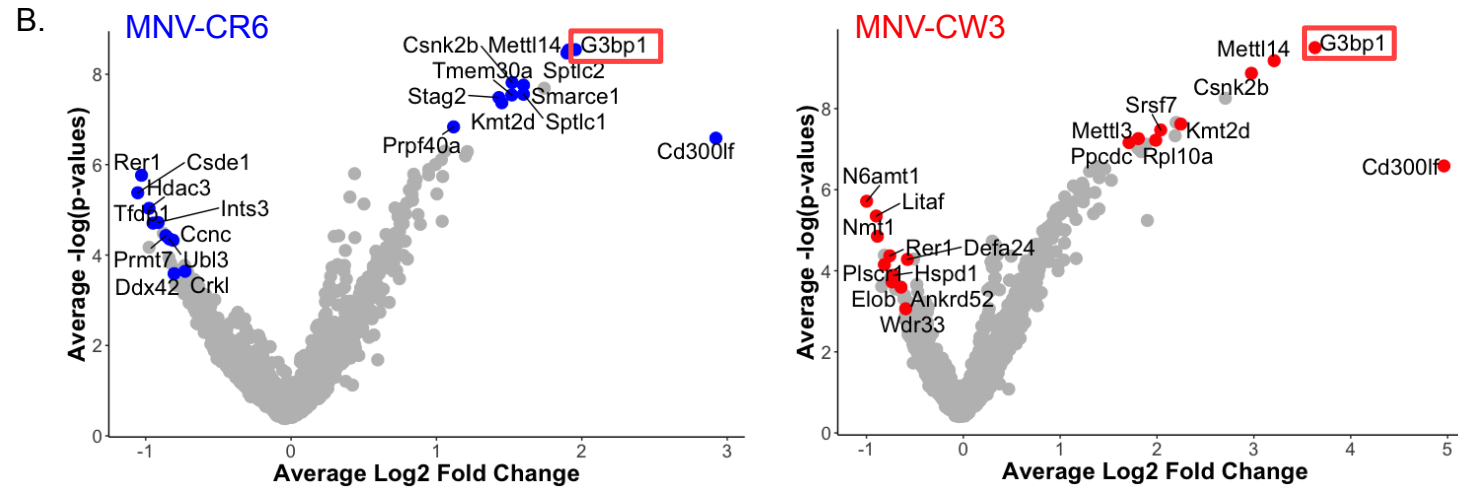
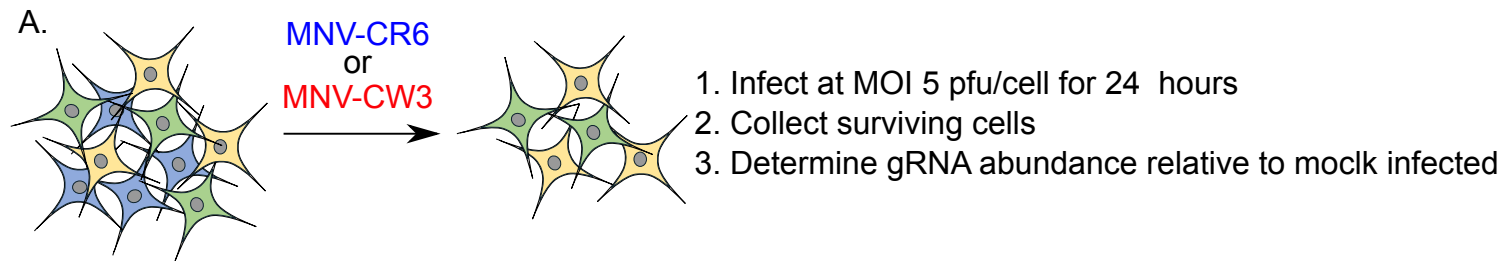
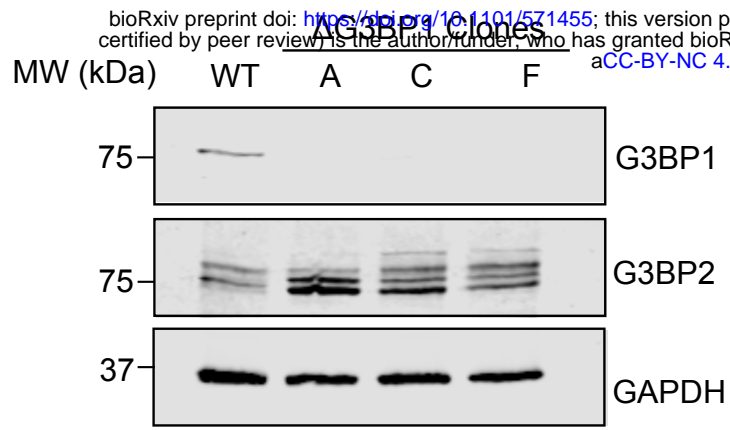
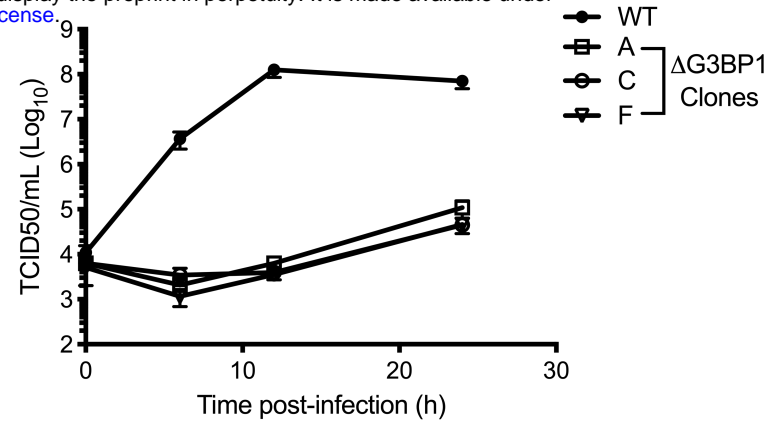


**Figure 4**

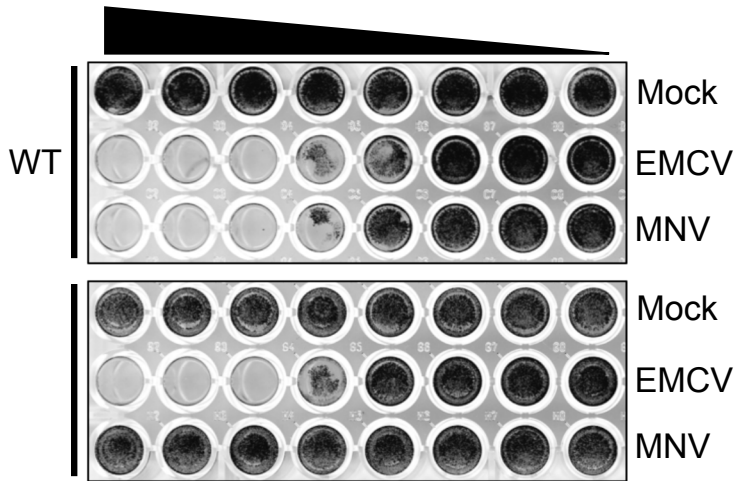
A.



B.



C.



D.

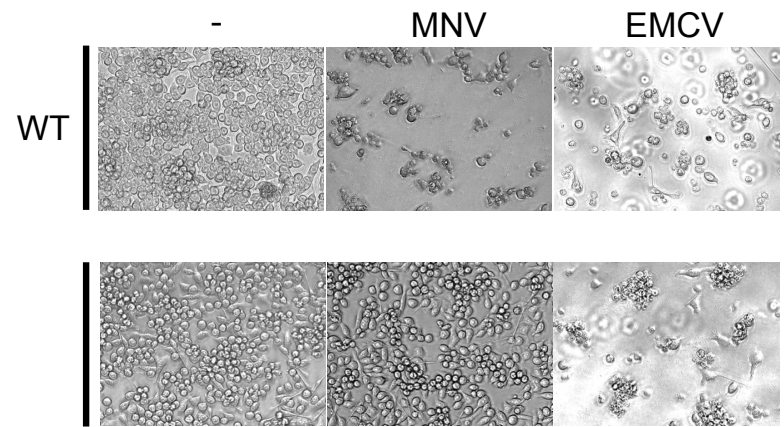
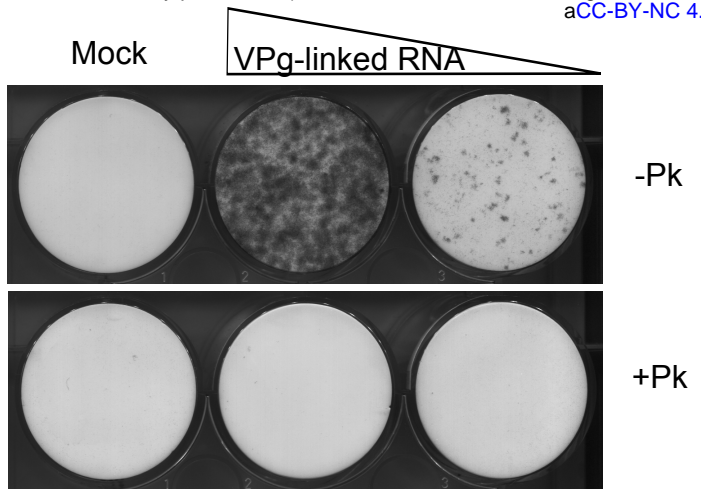


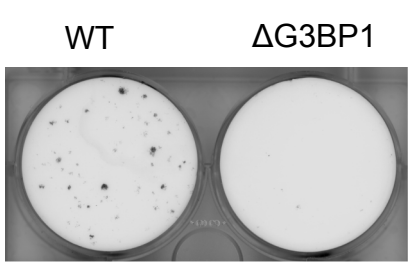
# Figure 5

A.

bioRxiv preprint doi: <https://doi.org/10.1101/571455>; this version posted March 8, 2019. The copyright holder for this preprint (which was not certified by peer review) is the author/funder, who has granted bioRxiv a license to display the preprint in perpetuity. It is made available under aCC-BY-NC 4.0 International license.



B.



C.

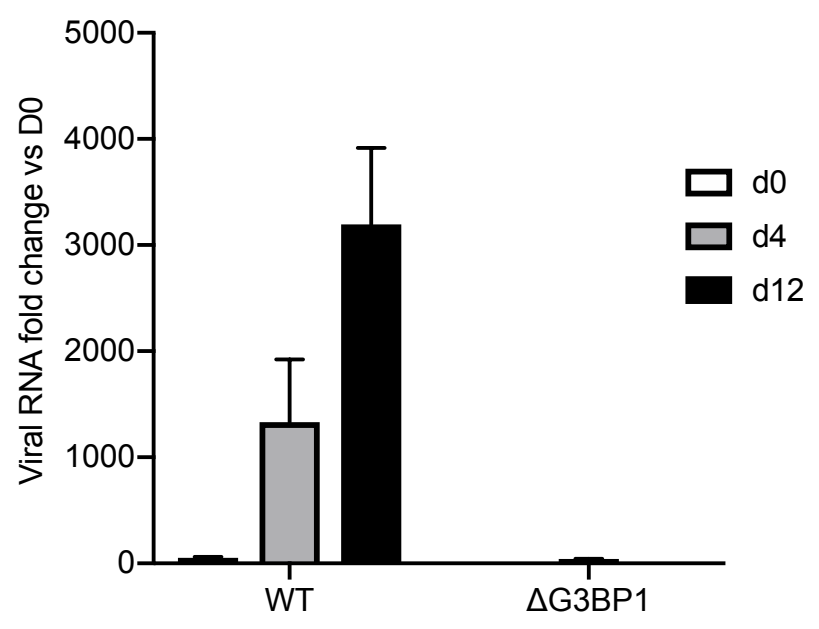
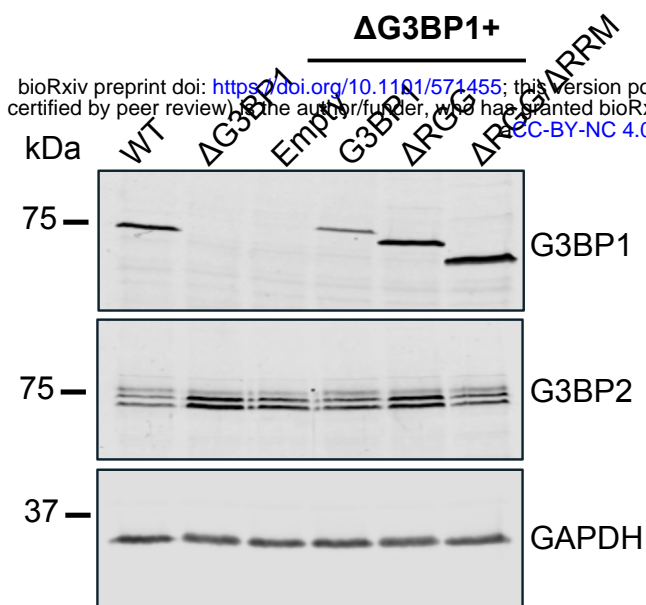
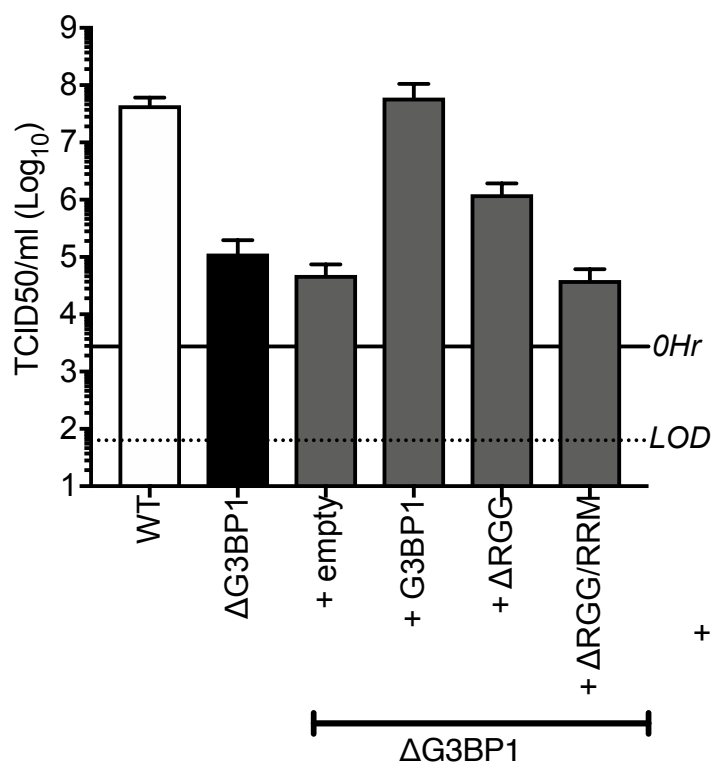


# Figure 6

A.



C.



B.

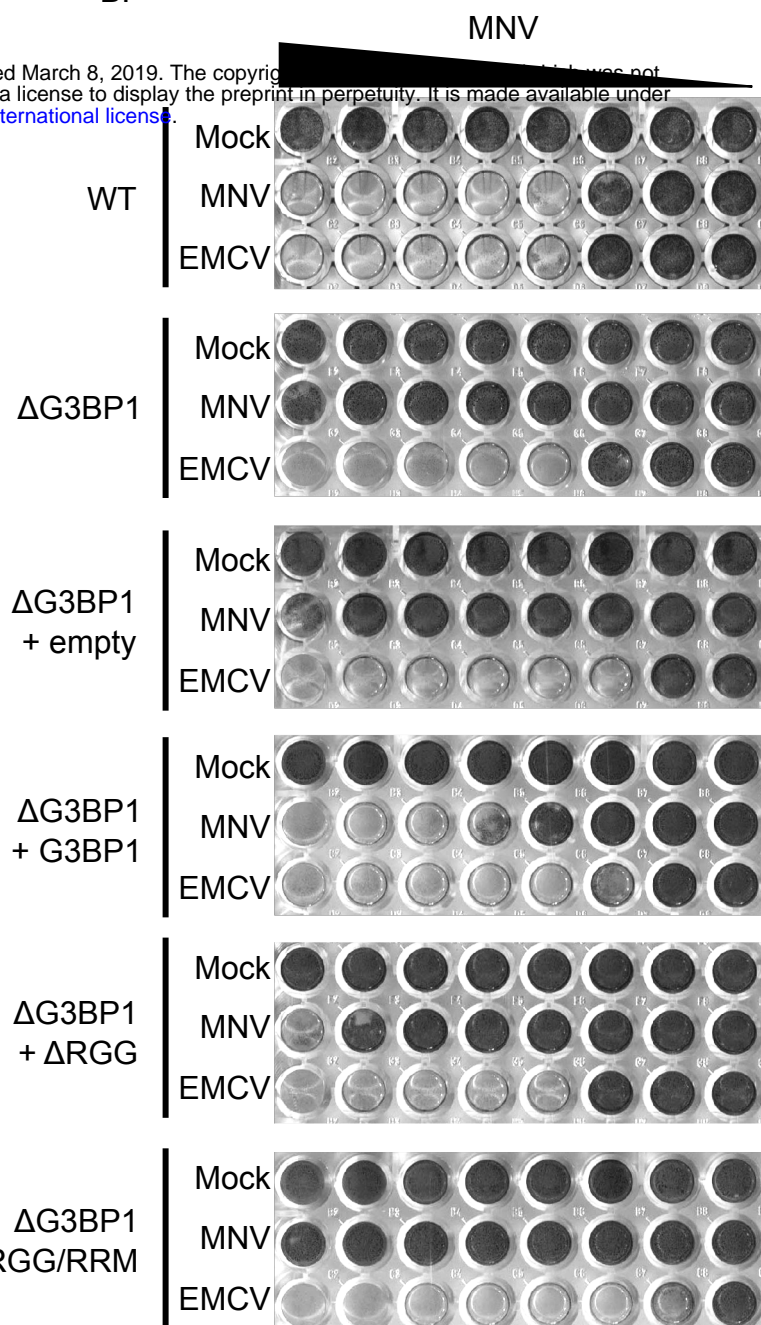
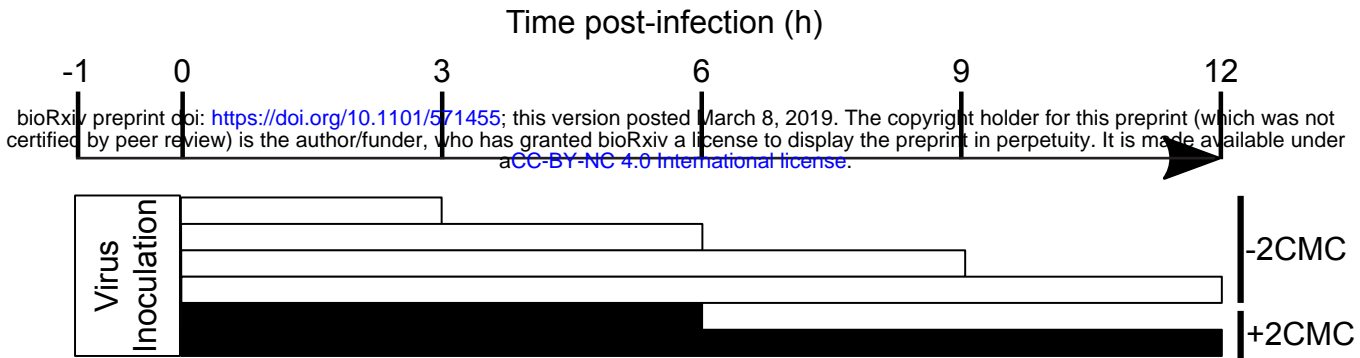


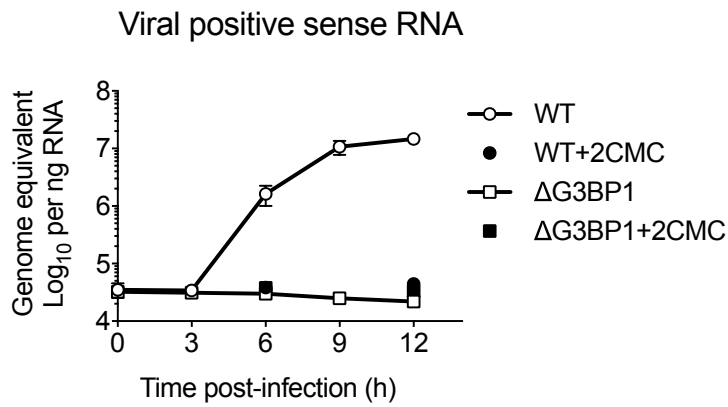


**Figure 8**

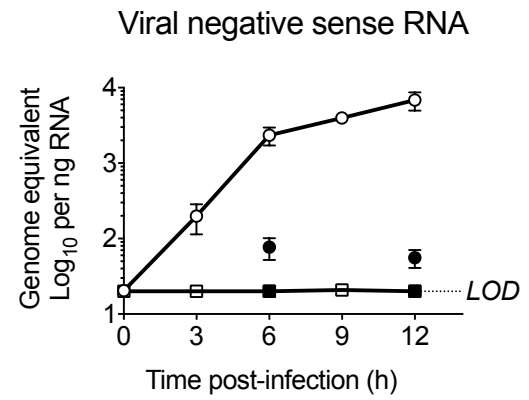
A.



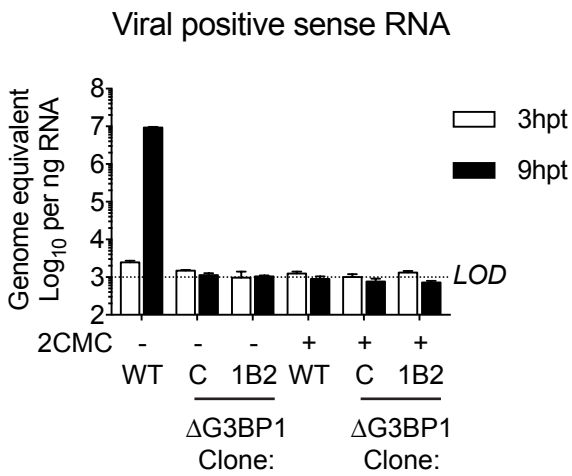
B.



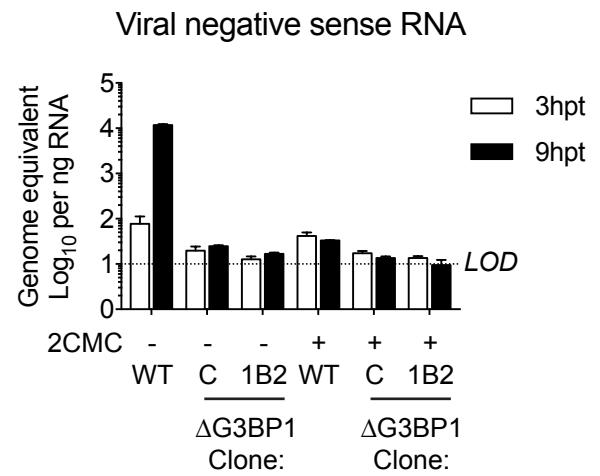
C.



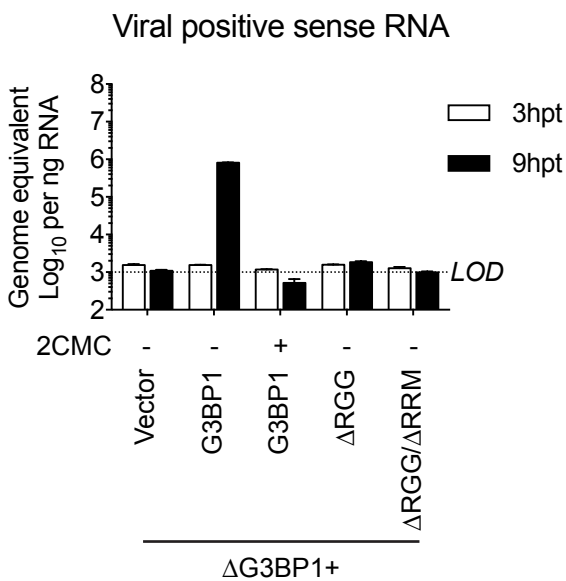
D.



E.



F.



G.

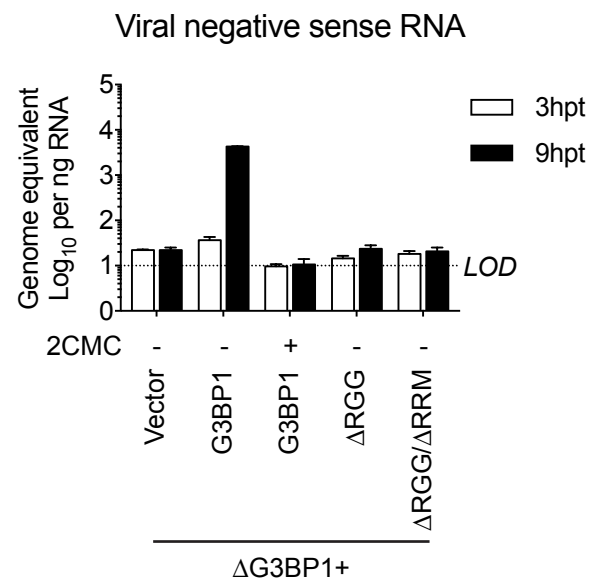


# Figure 9

A. bioRxiv preprint doi: <https://doi.org/10.1101/571455>; this version posted March 8, 2019. The copyright holder for this preprint (which was not certified by peer review) is the author/funder, who has granted bioRxiv a license to display the preprint in perpetuity. It is made available under aCC-BY-NC 4.0 International license.

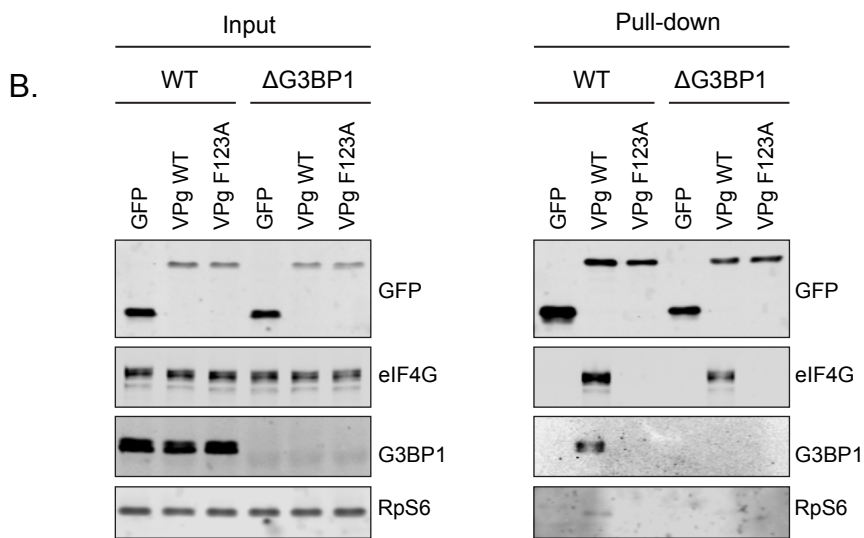
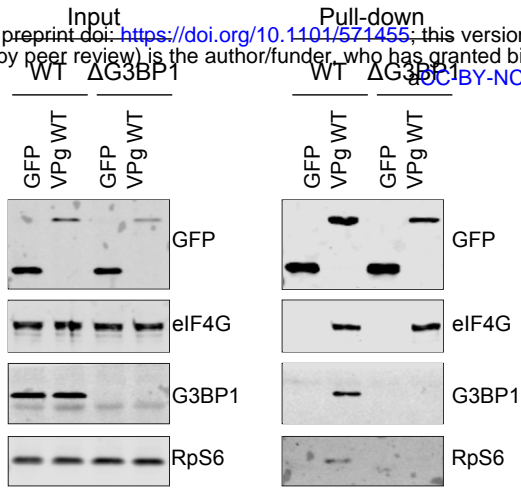




**Figure 10**

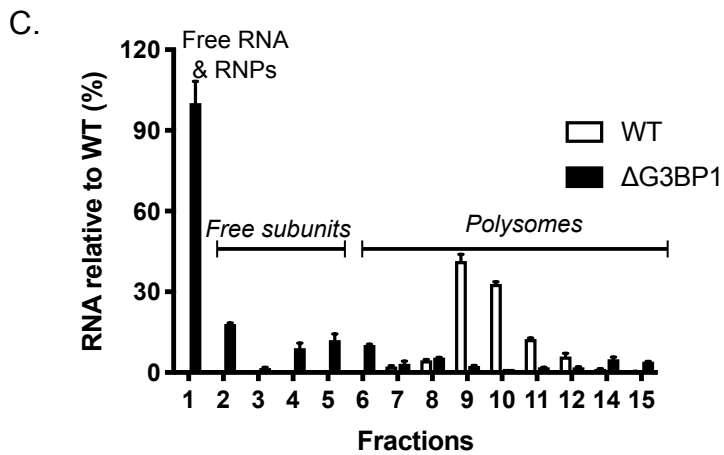
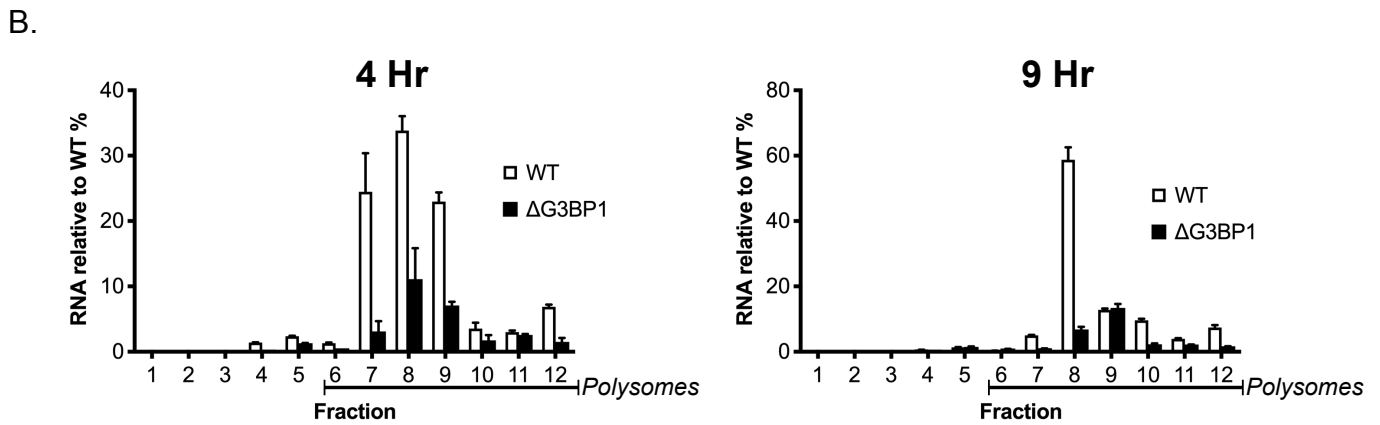
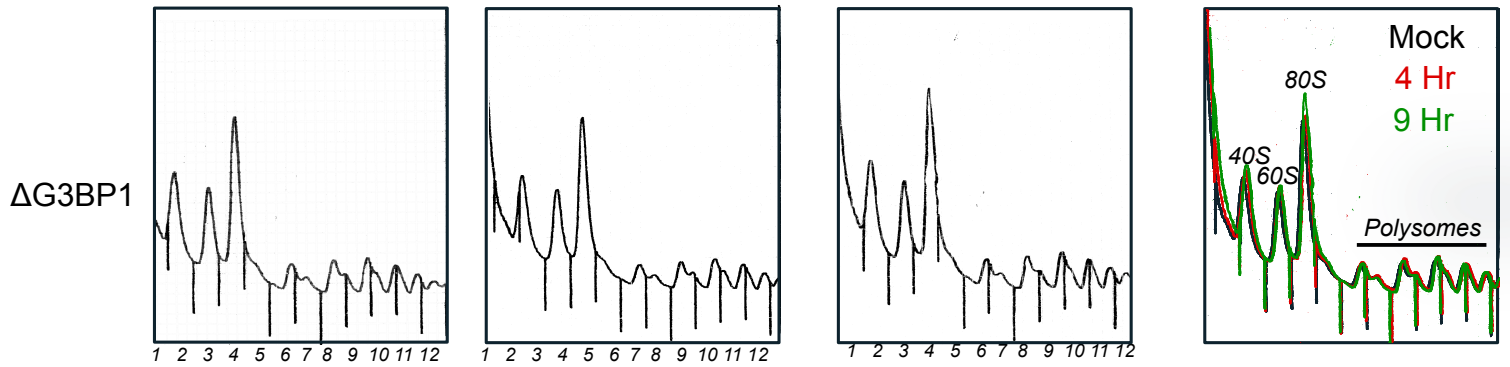
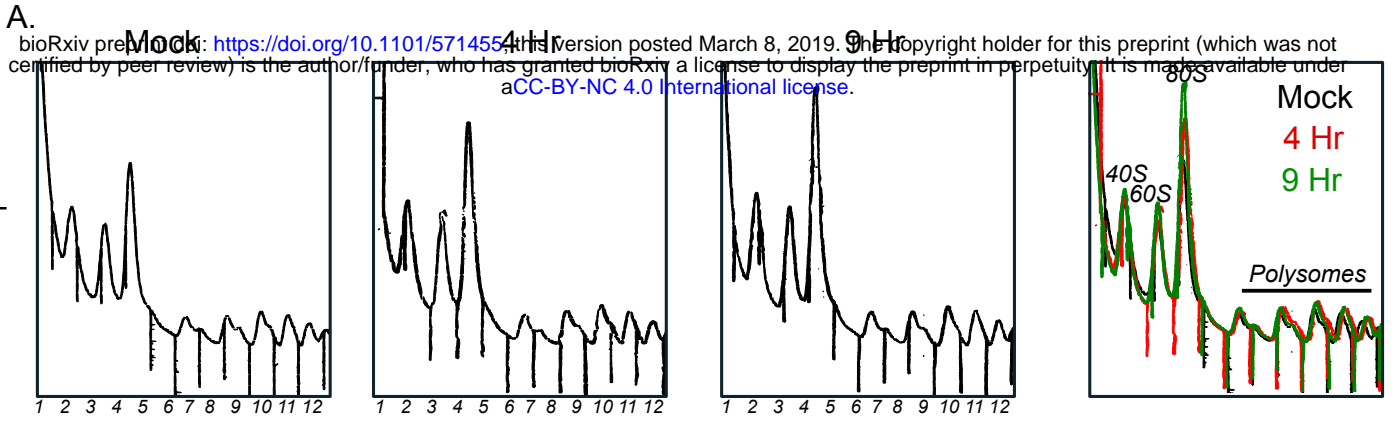
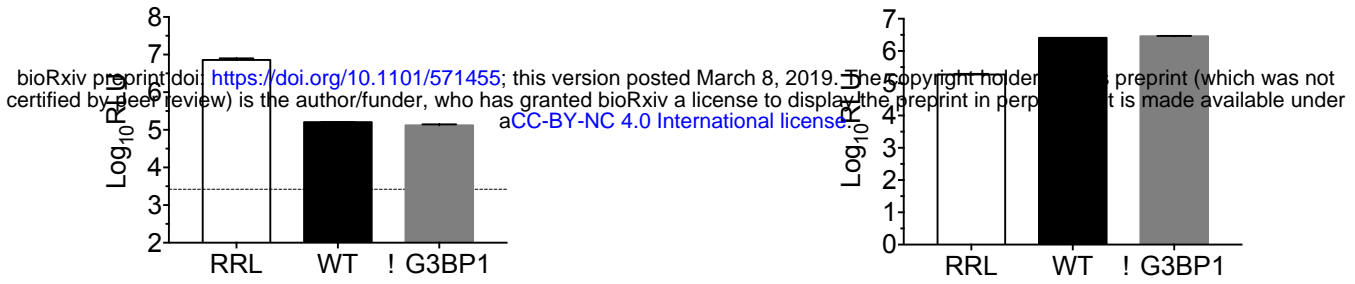
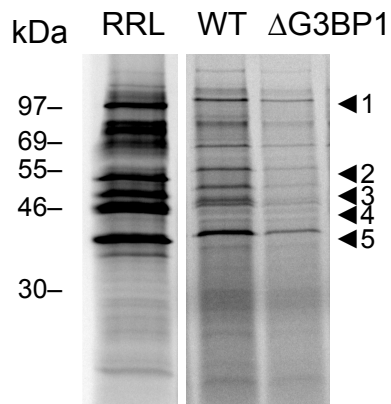


**Figure 11**

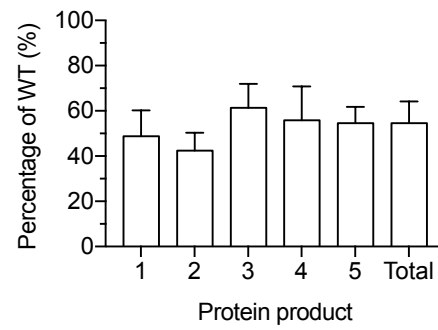
A.



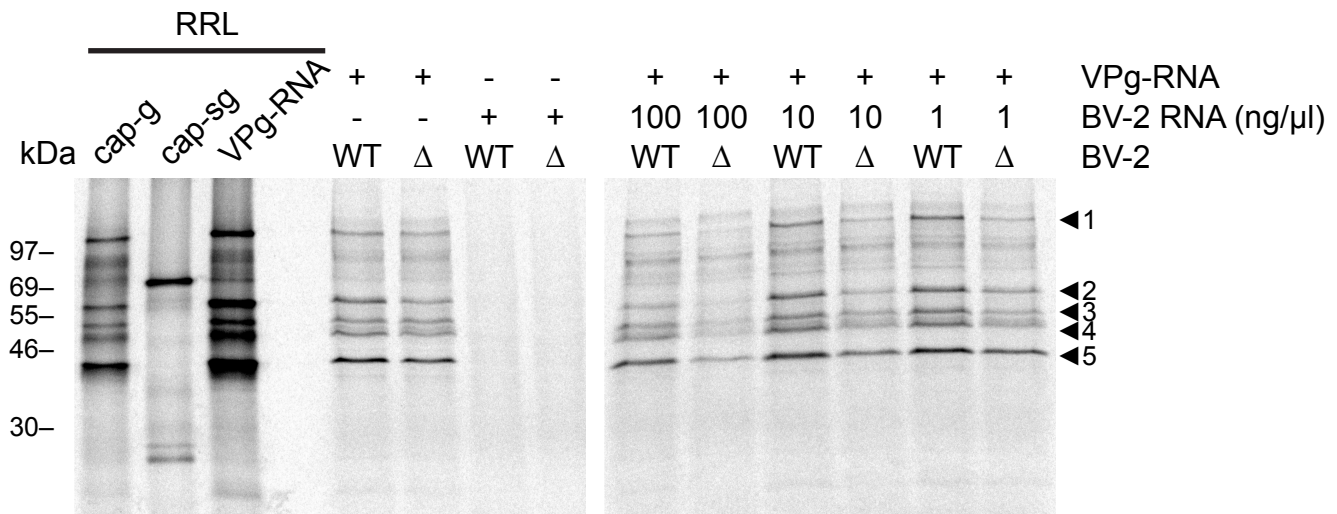
B.



C.



D.



E.

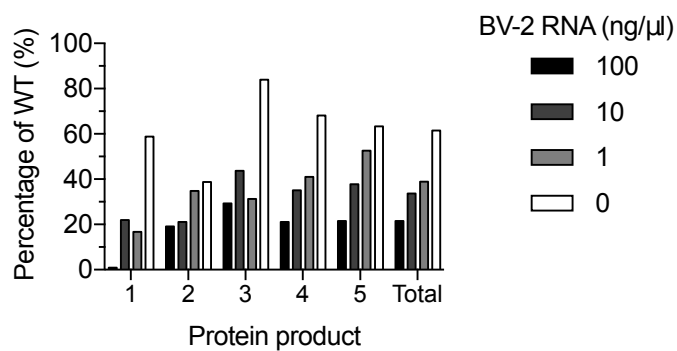


# Figure S11

